LSR Targets YAP to Modulate Intestinal Paneth Cell Differentiation

Yanan An[#1], Chao Wang[#1], Baozhen Fan[#2], Ying Li[1], Feng Kong[3,4,5], Chengjun Zhou[6], Zhang Cao[7], Jieying Liu[1], Mingxia Wang[1], Hui Sun[1], Shengtian Zhao[*2,3,4], Yongfeng Gong[*1]

Author affiliation:
1 Department of Physiology, Binzhou Medical University, Yantai, Shandong, CHINA
2 Department of Urology, Binzhou Medical University Hospital, Binzhou, Shandong, CHINA
3 Shandong Provincial Engineering Laboratory of Urologic Tissue Reconstruction, Jinan, Shandong, CHINA
4 Department of Urology, Shandong Provincial Hospital Affiliated to Shandong First Medical University, Jinan, Shandong, CHINA
5 Department of Central Laboratory, Shandong Provincial Hospital Affiliated to Shandong First Medical University, Jinan, Shandong, CHINA
6 Department of Pathology, The Second Hospital, Cheeloo College of Medicine, Shandong University, Jinan, Shandong, CHINA
7 Department of Pathology, Binzhou Medical University Hospital, Binzhou, Shandong, CHINA

[#] These three authors contributed equally to this work

* Corresponding authors:
Yongfeng Gong, MD, PhD, Professor
Department of Physiology
Binzhou Medical University
346 Guanhai Avenue
Yantai, Shandong, CHINA 264003
Phone: +86-535-6913163, +86-18705439006
E-mail: ygong@bzmc.edu.cn

Shengtian Zhao, MD, PhD, Professor
Department of Urology
Binzhou Medical University Hospital
661 Huanghe 2nd Road
Binzhou, Shandong, CHINA 256603
Phone: +86-543-3256802, +86-15153169567
E-mail: zhaoshengtian@sdu.edu.cn

Abstract

Lipolysis-stimulated lipoprotein receptor (LSR) is a multi-functional protein that is best known for its roles in assembly of epithelial tricellular tight junctions and hepatic clearance of lipoproteins. Here, we investigate the function of LSR in intestine biology. By using multiple conditional deletion mouse models and *ex vivo* cultured organoids, we find that LSR elimination in intestinal stem cells results in disappearance of Paneth cell without affecting the differentiation of other cell lineages. Mechanistic studies reveal that LSR deficiency increase abundance and nuclear localization of YAP by modulating its phosphorylation and proteasomal degradation. Intestinal LSR-deficient mice are susceptible to development of necrotizing enterocolitis. In addition, LSR can sense and interpret fatty acid signals derived from dietary lipids and transduce into inactivation of YAP. Thus, this study identifies LSR as an upstream negative regulator of YAP activity and part of the mechanism mediating connection between fat diet and YAP signaling in intestine.

Introduction

Lipolysis-stimulated lipoprotein receptor (LSR), a multi-functional type I transmembrane protein containing an immunoglobulin-like domain (Konno et al., 2020; Masuda et al., 2011), has been linked to a variety of biological processes, molecular functions and cellular compartments. In the liver, LSR recognizes apolipoprotein B/E-containing lipoproteins in the presence of free fatty acids, and is thought to be involved in the hepatic clearance of triglyceride-rich lipoproteins (Narvekar et al., 2009; Yen et al., 1994; Yen et al., 1999). LSR also plays an essential role in organization of tricellular tight junctions that are involved in epithelial barrier function (Masuda et al., 2011; Sugawara et al., 2021). In the brain, LSR is specifically expressed at tricellular tight junctions between central nervous system endothelial cells and plays critical roles for proper blood–brain barrier formation and function (Sohet et al., 2015). LSR is also a target molecule for cell binding and internalization of Clostridium difficile transferase (Hemmasi et al., 2015; Papatheodorou et al., 2011). Although its role as either a tumor promoter or suppressor (or

both) is not established, expression and localization of LSR have been found to be altered in several cancers (Dong et al., 2022; Shimada et al., 2017; Takahashi et al., 2021). The dominant subcellular localization of LSR is on the membrane, however, its localization in the nucleus of human epithelial cells has been reported (Reaves et al., 2017). Taken together, these findings suggest that the subcellular localization, function, and signaling pathways regulated by LSR are tissue- and cell type-specific. However, the specific cell types that express LSR have been difficult to identify, and the functions of LSR in postnatal development and tissue homeostasis have been hampered by the perinatal lethality of *Lsr* null mice (Mesli et al., 2004; Sohet et al., 2015).

Previous studies have revealed that LSR is highly expressed in the intestinal epithelium and localized at the basolateral membrane in addition to tricellular tight junctions of mouse intestine (Sugawara et al., 2021). *In vitro* studies in cultured EpH4 mouse mammary epithelial cells and Madin-Darby Canine Kidney (MDCK) cells indicates that LSR plays essential roles in the plasma membrane seal at tricellular tight junctions and in epithelial barrier function (Masuda et al., 2011; Sugawara et al., 2021). However, roles of LSR in intestinal homeostasis *in vivo* remain to be fully elucidated. Earlier work in Drosophila has established a pivotal link between tricellular tight junction proteins, stem cell behaviour, and intestinal homeostasis (Resnik-Docampo et al., 2017), to what extent this connection is conserved in mammalian systems remains uncertain. Meanwhile, embryonic lethality in LSR-deficient mice highlights the importance of LSR for development (Mesli et al., 2004), but the significance and relevance of this protein in regulating intestinal development and differentiation in mammals are largely unclear. It is also unclear whether LSR can transduce dietary signals and organismal nutritional status into regulation of intestinal homeostasis, given that it is located near the apical part of the epithelium and in contact with the intestinal lumen.

Here, we used a combination of *in vivo* conditional deletion mouse models and *ex vivo* cultured organoids to investigate the role of LSR in the regulation of intestinal homeostasis. We show that absence of LSR in intestinal stem cells (ISCs) affects the development of Paneth cells in small intestine by regulating protein abundance and localization of YAP. An *ex vivo* organoid-forming assay showed that intestinal crypts from *Lsr* knockout mice or induced pluripotent stem cells (iPSCs) with stable *LSR* knockdown formed symmetrical spherical organoids without Paneth cell lineage. Mechanistically, LSR controls YAP

phosphorylation and proteasomal degradation by modulating the binding of YAP to 14-3-3 zeta and phosphatase protein phosphatase 2A catalytic subunit (PP2Ac). Moreover, the disease relevance of these findings was indicated by the striking susceptibility of epithelial-specific LSR-deficient mouse to the development of experimental necrotizing enterocolitis (NEC), a severe and often fatal disease that affects premature infants, and in which intestinal epithelial LSR was shown to be markedly decreased in mice and humans. Further, although the relationship between high fat diet (HFD) exposure and YAP activity has been established (Poon et al., 2013; Wang et al., 2020b; Yuan et al., 2017), the molecular basis associated with how fat diet affect YAP activity has not been thoroughly examined. This study discovered that fat diet component, such as palmitic acid (PA), potently inhibit YAP activity through LSR, which represents a novel regulatory pathway for YAP signaling with important implications for human responses to dietary constituents.

Results

LSR ablation results in increased numbers of proliferating cells and loss of Paneth cell lineage in the small intestine

LSR is widely expressed in small intestine and colon which suggested a role for LSR in regulating homeostasis in the gastrointestinal tract. To bypass the embryonic lethality of constitutive deletion and investigate the potential role of *Lsr* in intestinal homeostasis, we generated $Lsr^{loxP/loxP}$ mice, in which the mutant Lsr allele contains exons 1~2 flanked by loxP sites, on a C57BL/6J background (Fig. S1A). We used $Lsr^{loxP/loxP}$*;CAG-CreER* mice to achieve global *Lsr* deletion ($Lsr^{-/-}$) upon tamoxifen treatment initiated at 7–8 weeks of age. We also generated intestinal-epithelium-specific *Lsr*-deficient mice ($Lsr^{vill\ KO}$) by intercrossing *villin-Cre* and $Lsr^{loxP/loxP}$ mice (Fig. S1B). qRT-PCR and western blot analysis of LSR expression showed that the transcription and expression of LSR in the intestines of $Lsr^{vill\ KO}$ and $Lsr^{-/-}$ mice were successfully blocked (Fig. 1, A-D). LSR has been previously reported to be localized at both the basolateral membrane and tricellular tight junctions (Sugawara et al., 2021), we found that LSR was expressed throughout the cellular membrane of epithelium in confocal sections, and did not show remarkable concentration at tricellular tight junctions in the Lsr^{ctrl} mouse intestine (Fig. 1E). This was further ascertained by the disappearance of LSR signal in intestinal epithelium of $Lsr^{vill\ KO}$ and $Lsr^{-/-}$ mice

118 (Fig. 1, E and F). In addition, transmission electron microscopy (TEM) showed that the structure of tight
119 junctions between the intestine epithelial cells (IECs) in $Lsr^{vill\ KO}$ mice was not significantly different
120 from that in Lsr^{ctrl} mice (Fig. S1C). Further immunostaining of ZO-1 and CLDN1, as an indicator of
121 bicellular tight junctions' integrity, showed no difference between $Lsr^{vill\ KO}$ and Lsr^{ctrl} small intestine (Fig.
122 S1, D and E). The tricellular tight junctions' integrity, assessed by tricellulin localization which was
123 detected as dots at tricellular tight junctions, remained intact in $Lsr^{vill\ KO}$ small intestine (Fig. S1F).
124 Together, these results indicate that the gross barrier function of tight junctions is not affected by the
125 deletion of LSR in IECs.

126 LSR deficiency had no effect on the overall structures of small intestine or colon (Fig. 1, G and H).
127 Surprisingly, the small intestines of $Lsr^{vill\ KO}$ mice were significantly thicker than those of Lsr^{ctrl} mice,
128 and this phenomenon was consistent at various times during the growth of mice (Fig. 1, G, I and J).
129 Moreover, we observed significantly longer villi in H&E-stained sections of small intestine of $Lsr^{vill\ KO}$
130 and $Lsr^{-/-}$ mice (Fig. 1, K and L). We speculated that there could be a considerable increase in proliferative
131 cell numbers in the *Lsr* mutant mice. Immunofluorescence was used to analyze the proliferation-related
132 proteins Ki67 and proliferating cell nuclear antigen (PCNA) in the small intestine, and the expression of
133 Ki67 and PCNA in the duodenum, jejunum and ileum was found to be significantly increased in Lsr^{vill}
134 ^{KO} mice (Fig. 2, A and B). Western blot analysis of Ki67 and PCNA confirmed this result in $Lsr^{vill\ KO}$ and
135 $Lsr^{-/-}$ mice (Fig. 2, C and D). To address if ISCs are responsible for the proliferation in small intestine,
136 we performed qRT-PCR and immunofluorescence analysis for olfactomedin 4 (OLFM4), a marker
137 expressed by the $Lgr5^{+}$ ISCs. Absence of LSR did not change OLFM4 expression of the small intestine
138 (Fig. 2, E and F and Fig. S1G), indicating that the highly proliferating cells in $Lsr^{vill\ KO}$ and $Lsr^{-/-}$ mice
139 were not ISCs. Since an increased percentage of Ki67 positive cells was predominantly found in the
140 transit-amplifying zone (Fig. 2A), we speculated that the proliferating cells may be undifferentiated
141 progenitor cells. In summary, these data demonstrate that in the absence of LSR, ISCs do not contribute
142 to the population of proliferating cells, presumably representing the transit-amplifying population leading
143 to increased villus length.

144 In agreement with histological observations, which indicated the absence of granule-containing cells in
145 H&E-stained sections of small intestine of $Lsr^{vill\ KO}$ and $Lsr^{-/-}$ mice (Fig. 1, K and L), RNA sequencing

146 (RNA-seq) analysis of small intestinal lysate from in $Lsr^{vill\ KO}$ and Lsr^{ctrl} showed that *Lsr*-knockout
147 downregulated many genes comprising the Paneth cell signature (*Lyz1, Itln1, Mptx2, Defa5,* and *Cd24*)
148 (Fig. 2, G and H) and DEFA family members (Fig. S1H). Data were validated by immunofluorescence
149 (Fig. 2, I and K) and qRT-PCR (Fig. 2J and Fig. S1I) performed on the small intestine from $Lsr^{vill\ KO}$,
150 $Lsr^{-/-}$ and control littermates. These results demonstrated that LSR elimination in intestinal epithelium
151 leads to depletion of Paneth cells. Despite the absence of Paneth cells, expression levels of markers for
152 other types of cells (EpCAM for IECs, MUC2 and SPDEF for goblet cells, CHGA and NEUROG3 for
153 enteroendocrine cells, CDX1 and CDX2 for columnar absorptive cells, and LGR5 for stem cells) and
154 Periodic acid–Schiff (PAS) staining of the goblet cells were not significantly changed (Fig. 2, L and Fig.
155 S1, J-M). These data collectively suggest that LSR is absolutely required to maintain the Paneth cell
156 lineage.

157 **LSR is required for $Lgr5^+$ ISCs to Paneth cell differentiation**

158 Paneth cells, like all other intestinal epithelial cell types, can be derived from $Lgr5^+$ ISCs, we conjectured
159 that LSR might affect the function of $Lgr5^+$ ISCs to differentiate into Paneth cells. Interestingly, we found
160 that LSR was highly expressed in $Lgr5^+$ ISCs at the bottom of intestinal crypts (Fig. 3A). These results
161 suggested that LSR may affect the function of $Lgr5^+$ ISCs, thereby making them lose the ability to
162 differentiate into Paneth cells. We used a *Lgr5-CreERT2* strain to selectively delete *Lsr* in $Lgr5^+$ ISCs in
163 a tamoxifen-inducible manner (hereafter referred to as $Lsr^{ISC\ KO}$) and to specifically explore the cellular
164 and molecular consequences of *Lsr* deletion in $Lgr5^+$ ISCs (Fig. 3, B and C). Although the lifespan of
165 Paneth cells is estimated to be 30 days (Bjerknes and Cheng, 1981), qRT-PCR and immunofluorescence
166 staining revealed reduced expression of Paneth cell markers (Lyz1, Itln1, Mptx2, Defa5, and Cd24a) in
167 the small intestine of $Lsr^{ISC\ KO}$ mice 15 days after the last dosage of tamoxifen injection, again supporting
168 the idea that LSR is required for $Lgr5^+$ ISCs to Paneth cell differentiation (Fig. 3, D and E). In line with
169 the findings in $Lsr^{vill\ KO}$ mice, $Lsr^{ISC\ KO}$ intestine possessed other intestinal cell types, such as IECs, ISCs,
170 enteroendocrine cells and goblet cells (Fig. S2, A and B). In $Lsr^{ISC\ KO}$ mice, intestinal permeability assay
171 showed that the concentration of FITC-Dextran 4000 in plasma seemed to increase compared to that of
172 the Lsr^{ctrl} mice, but it did not attain a significant difference (Fig. S2C), indicating the phenotype caused
173 by LSR deficiency is not attributable to the dysfunction of permeability barrier. In contrast to $Lsr^{vill\ KO}$

174 mice, we found no difference in the proliferative cells in small intestine of $Lsr^{ISC\ KO}$ mice, indicating a
175 potential direct role of LSR on transit-amplifying population. These results further demonstrated that in
176 the absence of LSR in $Lgr5^{+}$ ISCs, Paneth cells were not formed, but the differentiation of other IEC
177 types was unaffected.

178 We also took advantage of crypt organoid culture to confirm the findings. Immunofluorescence analysis
179 showed that LSR was expressed in organoid culture of Lsr^{ctrl} crypts and localized to the cell membrane,
180 while no LSR expression was observed in $Lsr^{vill\ KO}$ crypt organoids (Fig. 3F). As expected, most crypts
181 in Lsr^{ctrl} mice differentiated and budded into organoids with villi over time (Fig. 3G). However, when
182 intestinal crypts from $Lsr^{vill\ KO}$ mice were cultured, *Lsr* deletion resulted in the formation of symmetrical
183 spherical organoids (Fig. 3, F and G). In addition, on day 6, the shape of the spherical organoids did not
184 change significantly; and the number of organoids gradually decreased (Fig. 3, G-I).
185 Immunofluorescence staining showed that the distribution and quantity of stem cells (OFLM4) and
186 epithelial cells (EpCAM) in $Lsr^{vill\ KO}$ organoids were similar to those in Lsr^{ctrl} organoids (Fig. 3, J and
187 K). Interestingly, similar to the above *in vivo* results, the Paneth cell markers (LYZ1 and MPTX2)
188 exhibited significantly reduced and even complete loss of expression in $Lsr^{vill\ KO}$ organoids (Fig. 3, L and
189 M). Therefore, our results indicated that the Paneth cell number was positively correlated with the LSR
190 expression level in both the crypt organoids and the intestine. Although qRT-PCR showed that the levels
191 of the Paneth cell markers (*Mptx2, Itln1* and *Defa5*) were significantly reduced in $Lsr^{vill\ KO}$ organoids
192 (Fig. S2D), the numbers of other types of cells did not differ significantly between the $Lsr^{vill\ KO}$ and Lsr^{ctrl}
193 organoids (Fig. 3, N-P and Fig. S2E). Therefore, the organoid culture of *Lsr* deficient crypts truthfully
194 recapitulated the phenotype of $Lsr^{vill\ KO}$ mice intestine. Next, we knocked down *LSR* in human iPSCs
195 (Fig. 3Q) and then cultured organoids. Unsurprisingly, we obtained results similar to those described
196 above (Fig. 3, R-V), indicating a conserved function of LSR in the intestine from mouse to human.
197 Collectively, these findings support a critical role for LSR in regulating ISCs differentiation to Paneth
198 cells.

199 **Loss of LSR results in upregulation and activation of YAP**

200 In intestine, excessive YAP can inhibit the differentiation of ISCs into Paneth cells (Gregorieff et al.,

201 2015), and promote the proliferation of undifferentiated progenitor cells (Camargo et al., 2007). Recent
202 work by Serra *et al*. revealed that homogeneous activation or suppression of YAP abolished Paneth cell
203 differentiation and organoid budding, leading to the development of symmetrical spheres that were either
204 develop into enterocysts or remain as undifferentiated (Serra et al., 2019). The loss of Paneth cells,
205 proliferation of undifferentiated progenitor cells, and formation of symmetrical spherical organoids
206 resulting from elimination of *Lsr* in the intestine led us to test whether abnormal YAP activation
207 contributes to these phenotypes. Confocal imaging showed a distinct colocalization of YAP with LSR in
208 mouse intestine and Lgr5^{+} ISCs (Fig. 4A), indicating that LSR might have a regulatory effect on YAP.
209 Additionally, in Lsr$^{-/-}$, Lsr$^{vill\ KO}$ and Lsr$^{ISC\ KO}$ mouse models, we observed enhanced YAP protein
210 abundance accompanied by increased mRNA expression of the well-established YAP target genes, such
211 as *Edn1, Ctgf,* and *Cyr61 (Fan et al., 2022)*, in the small intestine (Fig. 4, B-G), but the mRNA expression
212 level of *Yap* did not change significantly (Fig. 4, E-G). To test directly whether elevated YAP contributes
213 to the phenotype caused by LSR deletion, we lowered YAP signaling in Lsr$^{vill\ KO}$ mice with verteporfin
214 (VP), a pharmacologic inhibitor of YAP-TEAD association, twice per day from postnatal day 7 to day
215 21. And then immunofluorescence staining of MPTX2 was performed to evaluate the content of Paneth
216 cells in small intestine. The expression of MPTX2 was found to be significantly increased in small
217 intestine of VP-treated Lsr$^{vill\ KO}$ mice (Fig. 4H). In addition, qRT-PCR showed that the mRNA levels of
218 Paneth cell markers (*Lyz1, Itln1, Mptx2* and *Defa5*) were significantly increased in VP-treated Lsr$^{vill\ KO}$
219 mice (Fig. S2F). These results indicated that VP treatment restored Paneth cell number. H&E staining
220 showed that the small intestinal villi hyperproliferation were also partially suppressed in VP-treated Lsr^{vill}
221 ^{KO} mice (Fig. 4I). The expression of several YAP target genes *Edn1, Ctgf* and *Cyr61* was significantly
222 suppressed by VP treatment (Fig. 4J), indicating decreased YAP signaling in intestine of VP-treated
223 Lsr$^{vill\ KO}$ mice. Similar results were observed in Lsr$^{vill\ KO}$ mice treated with lentiviruses carrying the *Yap*
224 shRNA (Fig. 4, K-M and Fig. S2G). These observations strongly support the causal link between the
225 LSR-dependent YAP regulation and the altered Paneth cell differentiation in *Lsr*-null mice.

226 Next, we sought to verify the importance of YAP to the phenotype of *Lsr*-deficient intestine. We
227 examined the expression of YAP in ISCs *in vitro*, and found that *Lsr* deletion led to significant increases
228 in YAP expression and nuclear translocation in the ISCs isolated from Lsr^{ctrl} and Lsr$^{ISC\ KO}$ mouse intestine
229 (Fig. 4N). Then the enhanced YAP expression and nuclear translocation were also observed in ISCs

230 isolated from the Lsr^{ctrl} and $Lsr^{vill\ KO}$ mouse intestine (Fig. S2H). Next, we verified the above results in
231 $Lsr^{vill\ KO}$ intestinal organoids by treating with YAP knockdown lentivirus according to a previously
232 described method (Goga et al., 2021). Briefly, 12 hours after budding was observed in the Lsr^{ctrl}
233 organoids, a timepoint YAP inactivation was observed (Gjorevski et al., 2022), $Lsr^{vill\ KO}$ organoids were
234 randomly divided into YAP knockdown virus treatment group and control virus treatment group. 5 hours
235 after virus transfection, organoids were seeded in Matrigel and cultured for 3 days before harvesting for
236 RNA isolation and immunofluorescence staining. The qRT-PCR showed that *Yap* shRNA lentiviral
237 transduction reduced the levels of *Yap* down to 30% in organoids (Fig. S2I), and rescued de novo crypt
238 formation (Fig. S2J) and normalized Paneth cell differentiation (Fig. S2K). Taken together, these results
239 confirmed a role for YAP activation in regulation of ISCs function downstream of LSR.

240 Wnt/β-catenin signaling pathway was discovered to be required for intestinal homeostasis and Paneth
241 cell differentiation (Totaro et al., 2018). However, β-catenin staining of crypts in the $Lsr^{vill\ KO}$ and Lsr^{ISC}
242 ^{KO} mice was similar to that of control crypts (Fig. S2, L and M). Activation of YAP has been reported to
243 directly inhibit Wnt signaling in the intestine (Cheung et al., 2020; Li et al., 2020), but LSR knockout
244 did not affect expression of most of the β-catenin-target genes including *Ccnd1, Axin2,* and *Cd44* in both
245 the intestinal tissue and $Lgr5^{+}$ ISCs isolated from $Lsr^{vill\ KO}$ and Lsr^{ctrl} mice (Fig. S2, N and O). This data
246 may be due to alterations in negative feedback mediators in the Wnt pathway. Further, both ATOH1 and
247 SOX9, two critical transcription factors for the differentiation of intestinal Paneth cell lineage, were not
248 significantly altered by *Lsr* ablation in ISCs (Fig. S2, P-R).

249 **14-3-3 zeta and PP2Ac are involved in the regulation of YAP by LSR**

250 The above data clearly indicate a role of LSR on YAP expression and activation, we examined in closer
251 detail whether Hippo pathway activity, which negatively regulates YAP, is perturbed by LSR ablation.
252 Immunoblot analysis indicated that LSR ablation actually led to up-regulation of phosphorylated large
253 tumor suppressor (p-Lats), a component of the mammalian Hippo pathway, which inhibits YAP nuclear
254 translocation and promotes its proteasomal degradation (Fig. S3, A and B). We conjectured that the
255 elevation of p-Lats1 is induced by YAP activation via a potential negative feedback mechanism.
256 Moreover, the increase of YAP protein level was not due to increased transcription, since *Yap* mRNA

257 was slightly decreased in the small intestine (Fig. 4, F and G). Since Hippo pathway cannot account for
258 YAP up-regulation, we speculated that *Lsr* deletion may affect the metabolism of YAP and cause its
259 protein level to increase. Therefore, a protein synthesis inhibitor (cycloheximide, CHX) and a proteasome
260 inhibitor (MG132) were used to determine the effect of LSR on YAP metabolism. The degradation rate
261 of YAP in the $Lsr^{vill\ KO}$ group was significantly lower than that in the Lsr^{ctrl} group after CHX treatment
262 (Fig. 5A). Moreover, MG132 blocked the turnover of YAP in the presence of CHX, and deletion of *Lsr*
263 had an effect similar to that of MG132 on blocking YAP turnover (Fig. 5B). Thus, YAP is degraded via
264 the proteasome pathway, and deletion of LSR might increase YAP accumulation by suppressing its
265 proteasomal degradation. Phosphorylation of YAP at Ser381 can increase its ubiquitination, ultimately
266 leading to proteasomal degradation (Zhao et al., 2010). Decreased phosphorylation of p-YAP at Ser381
267 (Fig. 5C), as well as decreased YAP ubiquitination (Fig. 5D) was observed in the ISCs isolated from
268 $Lsr^{vill\ KO}$ mice. These results demonstrated that *Lsr* knockout enhanced YAP stability by decreasing its
269 phosphorylation at Ser381, thereby blocking its ubiquitination and degradation.

270 We next sought to determine the molecular mechanism through which LSR regulate the phosphorylation
271 of YAP. We performed a mass spectrometry analysis of LSR immunocomplexes from ISCs. Results
272 from three experiments identified a list of 289 cellular proteins that specifically interact with LSR. We
273 focused on two 14-3-3 proteins, 14-3-3 zeta and 14-3-3 gamma, and two protein phosphatases, protein
274 phosphatase 1 catalytic subunit alpha (PPP1CA) and PP2Ac (Fig. 5E), because they have been reported
275 to participate in the regulation of YAP in multiple tissues (Hu et al., 2017; Meng et al., 2016; Qi et al.,
276 2015; Schlegelmilch et al., 2011; Sun et al., 2021; Yan et al., 2021). It is known that the turnover of YAP
277 is regulated through its phosphorylation and ubiquitination in a 14-3-3 dependent manner. Remarkably,
278 coimmunoprecipitation (co-IP) and immunoblot analysis of *in vivo* and *in vitro* samples confirmed that
279 14-3-3 zeta interacted with both YAP and LSR (Fig. 5F and Fig. S3C), but 14-3-3 gamma, PPP1CA, or
280 PP2Ac did not interact with YAP or LSR either *in vivo* or *in vitro* (Fig. S3, D-H and Fig. 5G). PPP1CA
281 and PP2Ac have been reported to be phosphatases that directly and effectively dephosphorylate YAP
282 (Ser381). An antagonistic and competitive interaction has been reported between PP2Ac and 14-3-3 for
283 the phosphorylation of YAP (Schlegelmilch et al., 2011). Hence, we tested whether deletion of LSR
284 results in an increased association of YAP with PP2Ac or PPP1CA. YAP interacted with PP2Ac instead
285 of PPP1CA and exhibited reduced binding to 14-3-3 zeta in the ISCs from $Lsr^{vill\ KO}$ mouse intestine (Fig.

286 5H and Fig. S3I) and HEK293 cells transfected with YAP, 14-3-3 zeta and PP2Ac expression plasmids
287 (Fig. S3J), while LSR and YAP did not seem to bind to PP2Ac in the ISCs from Lsr^{ctrl} mouse intestine
288 or HEK293 cells (Fig. 5G and Fig. S3H). Therefore, YAP could interact with 14-3-3 zeta and PP2Ac
289 respectively, and deletion of LSR might increase the interaction between YAP and PP2Ac by decreasing
290 the YAP/14-3-3 zeta association. To determine whether PP2Ac can efficiently dephosphorylate YAP
291 (Ser381), an *in vitro* phosphatase assay is performed in the presence of PP2Ac. The presence of PP2Ac
292 resulted in diminished YAP (Ser381) phosphorylation and YAP accumulation (Fig. 5I). These results
293 suggested that loss of *Lsr* leads to more efficient association of YAP with PP2Ac, which can potentially
294 dephosphorylate YAP at Ser381 and thereby decrease its degradation.

295 **Loss of *Lsr* exacerbates inflammation in a mouse model of NEC**

296 Paneth cells, which are enriched in the ileum, have a central role in preventing intestinal inflammation
297 (Adolph et al., 2013) and defects in Paneth cells are a hallmark of NEC. Infants who have developed
298 NEC have decreased Paneth cell numbers compared to age-matched controls (Coutinho et al., 1998), and
299 ablation of murine Paneth cells results in a NEC-like phenotype (Lueschow and McElroy, 2020;
300 Lueschow et al., 2018). We speculated that Paneth cell loss caused by LSR deletion may render the
301 immature small intestine susceptible to development of NEC. Hence, to evaluate the role of LSR in NEC,
302 we used 2,4,6-trinitrobenzenesulfonic acid (TNBS) to establish NEC models. Enteral administration of
303 TNBS in 14-day-old mouse pups induced NEC, as revealed by villus disruption, clear separation of
304 lamina propria and edema in the submucosa (Fig. S4A and Fig. 6A), increased mRNA levels of
305 proinflammatory factors, including *IL-1α, IL-2, IL-6, IFN-γ* and *TNF-α* (Fig. 6B), and increased
306 infiltration of inflammatory cells (macrophages and neutrophils) (Fig. S4, B and C and Fig. 6, C and D)
307 in small intestine of mice treated with TNBS in Lsr^{ctrl} mice. As expected, LSR expression was
308 significantly decreased in the small intestines of mice treated with TNBS (Fig. 6, E and F), and the
309 number of Paneth cells was also significantly reduced (Fig. S4, D and Fig. 6, G and H). Compared with
310 Lsr^{ctrl} mice, $Lsr^{vill\ KO}$ mice showed worsening intestinal injury, represented by more severe transmural
311 injury in the small intestine (Fig. S4E and Fig. 6I), increased mRNA levels of *IL-1α, IL-2, IL-6, IFN-γ,*
312 and *TNF-α* (Fig. 6J), and increased infiltration of macrophages and neutrophils (Fig. S4, F and G and
313 Fig. 6, K and L) after NEC induction. Collectively, these results implied that the lack of LSR led to more

314 severe NEC. To further explore the effect of LSR on NEC, we used an AAV10 system with
315 intraperitoneal injection, which has been proven to primarily transduce cells in the intestine, then
316 established the NEC model in mice transduced with AAV encoding mouse *Lsr* (AAV-*Lsr*) or control
317 vector (AAV-CTL). The LSR overexpression AAV decreased the severity of TNBS induced NEC as
318 indicated by histopathological analysis (Fig. S4H and Fig. 6M), suppressed cytokines production (Fig.
319 6N), decreased inflammatory cells infiltration (Fig. S4, I and J and Fig. 6, O and P), and preserved Paneth
320 cell number (Fig. 6, Q and R) in the small intestine of AAV-*Lsr* treated mice. These results suggest that
321 LSR protects against TNBS induced NEC through upregulation of Paneth cell. To further verify the role
322 of LSR in NEC, we tested intestinal samples from NEC patients. Compared with healthy control, patients
323 with NEC exhibited severe intestinal injury (Fig. 6S) and significantly reduced expression of LSR (Fig.
324 6T), especially in ISCs (Fig. 6U). Similar to previous reports (Underwood, 2012), infants with NEC have
325 significantly decreased numbers of Paneth cells compared to age-matched controls (Fig. 6V). These
326 results confirmed that LSR plays an important role in the development of NEC and is expected to be a
327 potential therapeutic target for NEC.

328 **LSR mediates the inhibitory effect of PA on YAP**

329 LSR has been described as a lipoprotein receptor activated by free fatty acid, with oleate and palmitate
330 were the most efficient (Mann et al., 1995). Next, we aim to identify if fatty acid could be a potential
331 extracellular signal which are able to modulate the activity of LSR in the intestine. HFD or PA, a main
332 component of the HFD, did not alter the expression of LSR in small intestine (Fig. 7, A-D). However,
333 we observed less abundant YAP and reduced expression of a subset of YAP target genes such as *Edn1,*
334 *Ctgf,* and *Cyr61* at the mRNA levels in small intestine from HFD and PA-treated mice compared to
335 controls (Fig. 7, E-H). Then we isolated the $Lgr5^{+}$ ISCs from mouse small intestine and incubated that
336 in serum-free medium supplemented with PA for 24 hours. Results demonstrated that PA reduced
337 expression of YAP (Fig. 7K), partially translocated YAP from the nucleus into cytoplasm (Fig. 7I), and
338 suppressed the expression of many of its target gene (Fig. 7J), indicating YAP inhibition. These data
339 suggest that PA can suppress YAP activity. Next, we examined whether the inhibitory effects of PA on
340 YAP are indeed mediated by LSR. In contrast to wild-type intestine, loss of LSR abrogated the HFD or
341 PA-driven downregulation of YAP and its target genes, *Edn1, Ctgf,* and *Cyr61* (Fig. 7, E-H). Then we

342 isolated the ISCs from the small intestine of Lsr^{ctrl} and $Lsr^{vill\ KO}$ mice and treated the cells with PA. LSR
343 deficiency attenuated the regulatory effect of PA on YAP protein abundance, as well as the reduction of
344 YAP target gene expression (Fig. 7, J and K). The results collectively indicate LSR may be able to sense
345 and interpret fatty acid signals derived from dietary lipids and transduce the inactivation of YAP.

346 **Discussion**

347 Although the abundant expression of LSR has been described in intestine (Mesli et al., 2004; Sugawara
348 et al., 2021), roles of this receptor in intestinal development, physiology and disease remain unclear. Here,
349 we generated multiple conditional deletion mouse models to identify roles for LSR in the intestinal
350 epithelium. We show that genetic ablation of *Lsr* in the intestinal epithelium results in increased numbers
351 of proliferating cells, as well as a reduction in Paneth cell lineage. We demonstrate that the numbers of
352 $Lgr5^{+}$ ISCs quantified by OLFM4 immunostaining displayed no significant difference between $Lsr^{vill\ KO}$
353 and control samples, suggesting that the associated increase in proliferating cells in $Lsr^{vill\ KO}$ crypts is
354 likely due to increased progenitor cell numbers. Strikingly, elimination of LSR from the intestinal
355 epithelial compartment results in the almost complete disappearance of Paneth cell lineage, but had no
356 effect on the number and distribution of other types of cells in the small intestine. The disappearance of
357 Paneth cell was reproduced in the tamoxifen-inducible $Lsr^{-/-}$ and $Lsr^{ISC\ KO}$ mice. An *ex vivo* organoid-
358 forming assay showed that intestinal crypts from $Lsr^{vill\ KO}$ mice or iPSCs with LSR knockdown formed
359 symmetrical spherical organoids without Paneth cell lineage, implying that LSR plays a key role in the
360 regulation of ISC function and differentiation toward Paneth cells in the intestinal epithelium.

361 YAP is a regulator of intestinal regeneration and ISCs fate (Gjorevski et al., 2022). We here show that
362 the loss of LSR causes an increased abundance and enhanced nuclear translocation of YAP in $Lsr^{vill\ KO}$
363 intestinal epithelium and in $Lsr^{ISC\ KO}$ ISCs. As for now, the molecular events and functional consequences
364 that follow YAP activation remain controversial (Barry et al., 2013; Cai et al., 2010; Cheung et al., 2020;
365 Gregorieff et al., 2015; Li et al., 2020; Zhou et al., 2011). Previous work has shown that overexpression
366 of YAP results in the enhanced proliferation of the stem cell compartment and loss of differentiated cell
367 types in the small intestine (Camargo et al., 2007). Mice deficient for Hippo components Mst1 and Mst2
368 exhibited an expansion of stem-like undifferentiated cells and the almost complete disappearance of all

369 secretory lineages, due to an increased abundance and enhanced nuclear translocation of YAP caused by
370 the loss of Mst1/Mst2 (Zhou et al., 2011). Recent studies by several group have demonstrated that
371 removal of Lats1/2, which caused the increase of YAP/TAZ expression and nuclear accumulation,
372 resulted in expansion of the transit-amplifying population (Guillermin et al., 2021; Li et al., 2020). In
373 agreement with these findings, the small intestine in $Lsr^{vill\ KO}$ mice was significantly thickened
374 accompanied by increased number of transit-amplifying cells. However, genetic ablation of *Lsr* only
375 resulted in loss of Paneth cell lineage, stem cells survived and produced the various cell types of intestinal
376 epithelium. Although Paneth cell development is tightly controlled by both Wnt and Notch pathways and
377 their downstream transcription factors, recent studies pointed out that spatial heterogeneities in YAP
378 activity are required for intestinal tissue morphogenesis, and homogeneous inhibitions or overexpression
379 of YAP in all cells reduces Paneth cell differentiation (Gjorevski et al., 2022; Li, 2019). We confirm this
380 finding and observe that homogeneous upregulation of YAP caused by LSR elimination from the
381 intestinal epithelial compartment results in the almost complete disappearance of Paneth cell lineage.

382 Loss of Paneth cells was confirmed in organoid cultures derived from *Lsr* knockout mouse crypts or
383 human iPSCs with stable *LSR* knockdown. Moreover, LSR deletion resulted in the formation of only
384 symmetrical spherical organoids from mouse crypts or human iPSCs. These phenotypes are similar to
385 YAP-overexpression organoids, where YAP is homogeneously active in all cells, and neither form Paneth
386 cells nor display symmetry breaking (Serra et al., 2019). Originally, the transcriptional regulator YAP
387 can stimulate single stem cells to enter a regenerative state and form a symmetric organoid (Serra et al.,
388 2019); then, the emergence of Paneth cells can break the symmetry of the organoid, followed by of
389 budding and the formation of villus structures (Chacon-Martinez et al., 2018; Sato et al., 2009). However,
390 if YAP is overexpressed and localized in the nucleus, the symmetry cannot be broken, and the organoid
391 remains spherical (Lukonin et al., 2020). Consistent with this concept, uniform induction in YAP activity,
392 which also abrogated spatial gradients in YAP activity, resulted in *Lsr* knockout organoids remain
393 symmetrical and contain no Paneth cells. Bearing in mind the pattern of YAP activity described above,
394 we reasoned that uniform inhibition of YAP by treatment with *Yap* shRNA lentivirus could not restore
395 the ability of *Lsr* knockout ISCs to differentiate into Paneth cells. Following YAP targeted knockdown,
396 however, we observed rescued de novo crypt formation and enhanced Paneth cell number in *Lsr* mutant
397 organoid. We do not currently know why such a difference exists. One possibility is that although

398 lentiviral transduction is a highly efficient method to introduce targeted gene in organoids, the number
399 of integrations per cell can be variable in organoids, resulting in heterogeneous knockdown efficiency of
400 YAP within the cell population.

401 Phosphorylated YAP is an inactive protein localized in the cytoplasm. When stimulated, YAP/TAZ are
402 dephosphorylated and translocate into the nucleus to regulate transcriptional activity (Oh and Irvine,
403 2009). Our study showed that LSR can affect the function of YAP by affecting its phosphorylation. A
404 previous study confirmed that the Ser381 of YAP is phosphorylated and further primes YAP for
405 phosphorylation by CK1d/e, after which it is ubiquitinated by $SCF^{\beta\text{-}TRCP}$ (an E3 ubiquitin ligase) and
406 degraded in the cytoplasm (Azzolin et al., 2014; Lapi et al., 2008; Maehama et al., 2021). Here, we
407 confirmed that LSR affects Ser381 phosphorylation of YAP. When *Lsr* is deleted, diminished YAP
408 degradation accounts for the increase in YAP abundance, in part or in whole.

409 14-3-3 proteins are a family of linker proteins widely distributed in eukaryotic cells that bind to hundreds
410 of phosphorylated proteins, playing a pivotal role in controlling signaling pathways and regulating the
411 subcellular localization of interacting proteins (Stevers et al., 2018; Xi et al., 2013). In intestine, 14-3-3
412 family proteins are likely an important part of machinery that regulates IEC differentiation, survival and
413 apoptosis during physiological and pathological conditions (Gomez-Suarez et al., 2016). Protein
414 phosphatase 2A (PP2A) is a major serine/threonine phosphatase ubiquitously expressed in eukaryotic
415 cells and involved in a plethora of cellular processes, including apoptosis, autophagy, cell proliferation,
416 and DNA repair (Dzulko et al., 2020). PP2A catalytic subunit (PP2Ac) is present in all forms of PP2A
417 and is an essential component of PP2A complexes activity (Zolnierowicz, 2000). 14-3-3 and PP2Ac
418 complexes compete for binding to target proteins, thereby regulating the subcellular localization of the
419 target protein and cellular activities (Paroni et al., 2008; Xi et al., 2013). Here, we found that binding of
420 LSR, 14-3-3zeta, and YAP resulted in the formation a stable complex, thus inhibiting the binding of
421 PP2Ac to YAP. When LSR was deleted, PP2Ac competitively bound to YAP and dephosphorylated it,
422 thus inhibiting its degradation and translocating it into the nucleus, where it exerted its effects on
423 transcriptional activity.

424 NEC is a life-threatening intestinal disease in premature infants (Weis et al., 2021), however, the

425 pathophysiology of NEC remains incompletely understood (Frost et al., 2017). Although NEC's
426 pathogenesis is multifactorial, Paneth cell depletion or dysfunction has been linked mechanistically to
427 development of NEC (Lueschow and McElroy, 2020). Our data clearly show that Paneth cell deficient
428 mice caused by *Lsr* depletion displayed increased susceptibility to TNBS induced NEC. We found that
429 the expression of LSR was significantly reduced in the intestines of NEC patients, and similar results
430 were also obtained in NEC mouse models. Systemic delivery of LSR using an adenoviral delivery system
431 profoundly inhibited the development and progression of NEC. These results reveal that LSR contributes
432 to intestinal injury and disease progression in NEC, which will potentially advance our understanding of
433 NEC, describe new biomarkers, and lead to novel therapeutic strategies for this multifactorial disease. It
434 would be interesting to investigate the contribution of LSR to other gut inflammatory disorders such as
435 Crohn's disease apart from NEC, because misfunctioning Paneth cells accelerate the progress of these
436 disorders (Wehkamp and Stange, 2020).

437 Fatty acid such as oleate acid and PA have been shown to be able to activate LSR (Bihain and Yen, 1992).
438 In addition to the importance of fatty acid as a metabolic energy source, it also plays important roles in
439 the regulation of stem cell proliferation and differentiation (Kang et al., 2014). PA has been shown to
440 both accelerate and augment gut mucosal recovery and growth after massive small bowel resection
441 (Sukhotnik et al., 2008). In support of a link between PA and stemness, is the observation that primary
442 organoids exposed *ex vivo* to PA possessed more $Lgr5^{+}$ ISCs and gave rise to more secondary organoids
443 compared to controls (Beyaz et al., 2016). On the other hand, a series of studies have established YAP as
444 nutrient sensors that integrate nutrient signals to growth regulation (Koo and Guan, 2018; Santinon et al.,
445 2016). HFD feeding results in a strong increase in nuclear localization of YAP/TAZ in white adipose
446 tissue which protects mature adipocytes from cell death during obesity (Wang et al., 2020a). PA can
447 inhibit YAP activity via inducing expression of MST1, which leads to suppression of endothelial
448 angiogenesis (Yuan et al., 2017). Here, we identified LSR mediated the HFD and PA-driven YAP activity
449 suppression in small intestine, indicating LSR may be able to connect nutrients to YAP activity by which
450 it contributes to intestinal homeostasis and certain pathological conditions. Moreover, it is possible that
451 the inhibitory effects of LSR activation on YAP activity are involved in the setting of a HFD impacts
452 tumor initiation and progression. Thus, these findings might further expand the connections between
453 metabolism and YAP. Although it has been proposed that the direct interaction of fatty acid with LSR

454 might cause a conformational shift to activate LSR (Mann et al., 1995), future research should be devoted
455 exploring whether fatty acid mediate its effects on YAP through direct interactions with the LSR or via
456 indirect mechanisms.

457 YAP signaling activity can be regulated by multiple factors, however, extracellular ligands, cell surface
458 receptors, and signaling pathways regulating YAP have not been thoroughly examined. Our results
459 demonstrate that LSR can directly impact the differentiation of ISCs into Paneth cells via regulating the
460 degradation of YAP in the ISCs (Fig.S5). This study establishes an important regulatory role of LSR in
461 restricting YAP activity, however, many questions remain. Are there additional direct or indirect effects
462 of LSR on YAP signaling activity? Are these tissue-specific or universal? Whether LSR can be used to
463 combat excess YAP activity? Intense studies are currently underway in our laboratory to address those
464 important questions.

465 **MATERIAL AND METHODS**

466 **Cell lines, plasmids, and antibodies**

467 Human HEK293 cells were obtained from ATCC (USA) and iPSCs were obtained from National
468 Collection of Authenticated Cell Cultures (China), and cultured according to the distributor's
469 recommendations. The expression plasmids containing mouse Lsr (pCMV6-LSR, NM_001164185,
470 MR225038), human LSR (pCMV6-LSR, NM_NM_205834, RC207960), mouse Yap (pCMV6-YAP,
471 NM_001171147, MR226049), mouse 14-3-3 zeta (pCMV6-14-3-3 zeta, NM_011740, MR203074),
472 mouse 14-3-3gamma (pCMV6-14-3-3 gamma, NM_018871, MR203103), mouse Ppp1ca (pCMV6-
473 Ppp1ca, NM_031868, MR204856), mouse PP2AC (pCMV6- Pp2ac, NM_019411, MR204384) genes,
474 and the knockdown plasmids containing YAP mouse shRNA plasmid (pGFP-C-shLenti, 22601) were
475 purchased from Origene Technologies (USA). The antibodies used in this study are summarized in
476 Supplemental Table 1.

477 **Animals**

478 All animals were housed in micro-isolator cages and received food and water freely. The laboratory

479 temperature was 24±1°C, and the relative humidity was 40-60%. The protocol in this study was approved
480 by the Committee on the Ethics of Animal Care and Use of Binzhou Medical University. The study was
481 conducted following the Guide for the Care and Use of Animals in Research of the People's Republic of
482 China. All animal studies were performed under isoflurane anesthesia, and every effort was made to
483 minimize suffering. C57BL/6J mice were obtained from Vital River Laboratory (China).

484 For the generation of $Lsr^{loxP/loxP}$ mice, targeting vector was constructed by inserting one SDA (self-
485 deletion anchor)-flanked neomycin cassette and two loxP sites flanking exons 1~2 of Lsr and then
486 electroporating into embryonic stem cells from C57BL/6J mice (conducted by Cyagen Biosciences Inc,
487 China). With one subsequent cross with C57BL/6J animals, the Neo transgene was removed and the
488 obtained $Lsr^{loxP/-}$ mice were then intercrossed in order to generate the $Lsr^{loxP/loxP}$ mice. $Lsr^{loxP/loxP}$ mice
489 were crossed with villin-Cre mice (Jackson Laboratory, 021504) (Madison et al., 2002), a mouse Cre line
490 that drives Cre recombination throughout the intestinal epithelium from embryonic day 12.5, to remove
491 Lsr from intestinal epithelium ($Lsr^{loxP/loxP}$/villin-$Cre^{+/-}$, $Lsr^{vill\ KO}$). Homozygous with villin-Cre negative
492 litter mates served as controls. $Lsr^{loxP/loxP}$ mice were crossed with *CAG-CreER* mice (Jackson Laboratory,
493 004682) (Hayashi and McMahon, 2002) to generate systemic *Lsr* knockout mice $Lsr^{loxP/loxP}$/*CAG-*$Cre^{+/-}$
494 ($Lsr^{-/-}$), homozygous with *CAG-Cre* negative litter mates served as controls. $Lsr^{loxP/loxP}$ mice were crossed
495 with *Lgr5-CreERT2* mice (GemPharmatech, T003768) to generate ISC-specific LSR knockout mice
496 ($Lsr^{loxP/loxP}$/Lgr5-$CreERT2^{+/-}$, $Lsr^{ISC\ KO}$), homozygous with *Lgr5-CreERT2* negative litter mates served as
497 controls. To induce the knockout of genes, tamoxifen suspended in corn oil was administered
498 intraperitoneally at a concentration of 10 mg/ml and dosed at 100mg/kg once every 24 hours for a total
499 of 5 consecutive days. 15 days post last tamoxifen injection, tissues were harvested for qRT-PCR,
500 Western blot, H&E or immunofluorescence staining analysis.

501 **Patient sample**

502 Human intestinal tissues were collected after approval by the Binzhou Medical University Review Board.
503 De-identified formalin-fixed paraffin-embedded tissue sections of NEC were compared with healthy
504 tissue margins resected for indications other than NEC (intestinal obstruction or spontaneous intestinal
505 perforation (n = 10). Written informed consent for research was obtained from donors before tissue

506 acquisition. The patients were from both sexes, between 4 and 49 days of born, and weighed between
507 0.9 and 1.15 kg.

508 **Intestinal permeability analysis**

509 Intestinal permeability was evaluated with fluorescein isothiocyanate (FITC)-Dextran 4000 (MCE, HY-
510 128868A, China) test. Briefly, mice were fasted for 6 h and then FITC-dextran 4000 (440 mg/kg body
511 wt) was administered by gavage. Blood was collected through tail vein 0h, 0.5h, 1h, 2h, 4h and 8h after
512 gavage, and serum was isolated. The analysis for the fluorescence intensity of FITC-dextran 4000 in
513 plasm was carried out with a multimode plate reader (PerkinElmer EnSpire Plate Reader, Waltham, MA,
514 USA) (excitation, 485 nm; emission, 520 nm). Standard curves for calculating the FITC-dextran
515 concentration were obtained by diluting FITC-dextran in PBS.

516 **TNBS-induced NEC**

517 2, 4, 6-Trinitrobenzene sulfonic acid (TNBS) were used to develop NEC (MohanKumar et al., 2012).
518 Briefly, TNBS was injected into 14-day-old C57BL/6J mice (n = 8) (50 mg/kg total body weight,
519 dissolved in 30% weight/volume ethanol by gavage and enema). Animals were monitored every 3h and
520 were euthanized if they developed signs of disease or at 48h using CO_2 inhalation followed by cervical
521 dislocation. Small intestine was harvested and processed for histological analyses. As previously
522 described (Namachivayam et al., 2020), intestinal injury was confirmed by histopathological grading and
523 was assigned by a blinded reviewer: grade 0 = no injury; grade 1 = mild injury: disruption of villus tips
524 or mild separation of lamina propria in the small intestine; grade 2 = moderate injury: villus disruption,
525 clear separation of lamina propria and/or edema in the submucosa; grade 3 = severe injury: transmural
526 injury in the small intestine. Others were collected for qRT-PCR and immunofluorescence analysis.
527 Control animals (n=8) received vehicle alone (30% ethanol).

528 **High fat diet and palmitic acid treatment**

529 High fat diet (containing 60% kcal from fats (Trophic Diet, TP23520, China)) was provided to Lsr^{ctrl}
530 mice and $Lsr^{vill\ KO}$ mice beginning at the age of 8 weeks and extending for a period of 4 months. Control

531 mice were sex and age-matched and fed with standard chow ad libitum.

532 The Lsr^{ctrl} mice and $Lsr^{vill\ KO}$ mice received an intragastric gavage of 0.2 ml 45% palmitic acid (MCE,
533 HY-N0830, China) dissolved in corn oil or corn oil alone. Mice were given 3 equally sized feedings daily
534 at 8:00 AM, 1:00 PM, and 6:00 PM. Gavage-fed animals were gradually adapted to this feeding regimen
535 for 5 days. At the end of day 5, mice were sacrificed 3 hours after the final gavage.

536 ***In vivo* administration of recombinant AAV**

537 AAVrh10 has been proved to be the most efficient rAAV serotype for intestine gene delivery (Polyak et
538 al., 2012). 7-day-old C57BL/6J mice received with 1×10^8 MOI virus genomic particles of Rh10-
539 pHBAAV-CMV-MCS-3flag-T2A-ZsGreen (AAV-CTL) or Rh10-pHBAAV-CMV-Lsr-3flag-T2A-
540 ZsGreen (AAV-*Lsr*) (prepared by Hanbio Biotechnology Inc, China) by intraperitoneal injection (n = 8).
541 1 week after transduction, mice were treated with TNBS to construct NEC models as described above.

542 To silence YAP *in vivo*, 1-week-old $Lsr^{vill\ KO}$ mice were injected intraperitoneally with a single dose of 2
543 $\times 10^8$ MOI particles of lentivirus/pHBLV-U6-MCS-CMV-ZsGreen-PGK-PURO (CTL) or
544 lentivirus/pHBLV-U6-YAP-siRNA-CMV-ZsGreen-PGK-PURO (*Yap* shRNA) (prepared by Hanbio
545 Biotechnology Inc, China) (n = 8). Mice were monitored every day for general wellbeing. 2 weeks after
546 transduction, mice were euthanized using CO_2 inhalation followed by cervical dislocation. Small
547 intestine tissues were harvested for RNA isolation and immunofluorescence and histological staining.

548 ***In vivo* administration of YAP inhibitor verteporfin**

549 1-week-old $Lsr^{vill\ KO}$ mice were injected intraperitoneally with verteporfin (100 mg/kg body weight)
550 every 2 days for 2 weeks, (n = 8). Mice were monitored every day for general wellbeing. After 2 weeks,
551 mice were euthanized using CO_2 inhalation followed by cervical dislocation. Small intestine tissues were
552 harvested for RNA isolation and immunofluorescence and histological staining.

553 **Histologic analysis**

554 Human and mouse intestine tissues were fixed overnight at 4°C in 4% paraformaldehyde and embedded

in paraffin. Intestine sections (5 μm thickness) were prepared by a routine procedure, then standard histological staining with H&E and periodic acid-Schiff (PAS). Transmission electron microscopy (TEM) was performed on glutaraldehyde-fixed, epoxy-embedded intestine samples and stained with uranyl acetate and lead citrate.

Immunofluorescence staining

The small intestine (duodenal, jejunal and ileal) cross sections were embedded in OCT. Small intestine cryosections (8 μm) were mounted onto glass slides, fixed in cold methanol or acetone for 20 min at -20°C. For immunofluorescence of mouse or human organoid, organoid on collagen I coated confocal dish were fixed with 4% paraformaldehyde. And then washed three times with PBS for 10 min each time, and blocked for 1 h at room temperature in 10% BSA diluted in PBS (containing 0.01% Tween 20). Then incubated overnight at 4°C with appropriate primary antibodies. Washed as before and incubated using FITC and/or rhodamine (TRITC) conjugated secondary antibodies (Invitrogen), followed by DAPI (Sigma) nuclear staining. And then sealed with ProLong™ Gold antifade reagent and analyzed using a confocal laser microscope (LSM 880 Basic Operation, Germany).

For human Paraffin section (5 μm thickness), immunostaining was preceded by antigen retrieval in EDTA buffer (pH 8.0), and blocked for 1 h at room temperature in 10% BSA. The primary antibodies were anti-human: LSR, MPTX2, OFLM4 and incubated overnight at 4°C. Then incubated with FITC and/or rhodamine (TRITC) conjugated secondary antibodies (Invitrogen) for 1.5 h at room temperature, followed by DAPI (Sigma) nuclear staining. The images were acquired using confocal laser microscope (LSM 880 Basic Operation, Germany).

RNA-sequencing (RNA-seq)

Total RNA was extracted using Trizol reagent (Invitrogen, 15596018) from intestine of Lsr^{ctrl} and $Lsr^{vill\ KO}$ mice at 4 weeks after birth. RNA-seq was performed on an Illumina Novaseq platform by Novogene (China). Paired-end clean reads were aligned to the mouse reference genome (Ensemble_GRCm38.90) with TopHat (version 2.0.12), and the aligned reads were used to quantify mRNA expression by using HTSeq-count (version 0.6.1). Differential expression analysis of two groups was performed using the

581 DESeq2 R package (1.16.1). The resulting P-values were adjusted using the Benjamini and Hochberg's
582 approach for controlling the false discovery rate. Genes with an adjusted *P-value <0.05* found by
583 DESeq2 were assigned as differentially expressed.

584 **Crypt and Lgr5^{+} ISCs isolation and culture**

585 Small intestines crypt cultures were prepared using previously described methods with modifications
586 (Gjorevski et al., 2016; Goga et al., 2021). In short, small intestines were first flushed with PBS, then cut
587 longitudinally. The tissue was chopped into 2-3 mm pieces, and further washed with cold PBS. The tissue
588 fragments were incubated in 5 mM EDTA-PBS solution on ice. Then EDTA was removed, the
589 supernatant fractions enriched for crypts were passed through a 70-micron strainer (BD Biosciences) to
590 remove the remaining cells of the intestinal villi fraction. The filtered fractions were then centrifuged to
591 collect the crypt fraction. Crypts isolated from the small intestine of Lsr$^{vill\ KO}$ and Lsr^{ctrl} mice was
592 resuspended into matrigel with DMEM/F12 medium (1:1 ratio) and plated into 24 well plates (Serra et
593 al., 2019). Crypt fraction organoids were kept in IntestiCult Organoid Growth Medium (STEMCELL
594 Technologies) with 100 μg/ml Penicillin-Streptomycin for amplification and maintenance.

595 For ISCs isolation, crypts were isolated from the small intestine of Lsr$^{vill\ KO}$ and Lsr^{ctrl} mice as described
596 previously in the methods. ISCs were isolated from the small intestine by immunomagnetic beads. In
597 short, the crypt suspensions were centrifuged and resuspended in undiluted TrypLE Express (Invitrogen)
598 supplemented with DNase I (2000 U/μl, Roche), and 10 μM Y27632 (MCE) and incubated at 37°C for
599 8min. Then, cold DMEM/F12 (STEMCELL Technologies) were added to the samples and triturated
600 twice, followed by centrifugated and resuspend the cell pellet in DMEM/F12. Positive selection of ISCs
601 were achieved using magnetic beads (1 μm diameter, Invitrogen) coated with a mouse monoclonal
602 antibody against LGR5 (invitrogen). For PA treatment, Lgr5^{+} ISCs isolated from mouse small intestine
603 were incubated in serum-free medium supplemented with 0.3 mM PA for 24 hours. And then cells were
604 harvested for RT-PCR, Western blot or immunofluorescence staining analysis.

605 **Lentivirus transduction of organoids**

606 For Lentivirus-Green-PURO-YAP (YAP-KD) virus infection experiments, cells recovery solution

607 (Corning) was used to harvest organoids and mechanically dissociated in Basal Media using a 10 ml
608 Pipette for 5-7 times up and down. Then, centrifuged the organoids at 250 × g for 5 min, 4°C, and
609 resuspend use 400 μl full growth medium containing 1×10^7 MOI YAP-KD Lentivirus, then add to 100
610 μl matrigel together. The mixture was incubated at 37°C for 5 h, mixing every 30 min. Later, the mixture
611 was centrifuged at 250 × g for 5 min at 4°C and organoids were seeded in matrigel and cultured for 3
612 days before harvesting for RNA isolation and immunofluorescence staining.

613 **shRNA molecular cloning, screening and retrovirus production**

614 The shRNA hairpin oligonucleotides, complementary to all the variants of human Lsr mRNA sequences
615 (NM_015925.7, NM_205834.4, NM_205835.4, NM_001260489.2, NM_001260490.2, and
616 NM_001385215.1) (Table S2), were synthesized by Sangon Biotechnology Inc, annealed, and cloned
617 into the moloney murine leukemia retrovirus vector pSIREN (Clontech), downstream of the human small
618 nuclear ribonucleoprotein U6 promoter to create the *LSR* shRNA constructs. Vesicular stomatitis virus
619 glycoprotein (VSV-G) pseudo typed retroviruses were produced in HEK293 cells and used to infect target
620 cells at a titer of 1×10^7 CFU/ml, as described previously (Gong et al., 2014).

621 **Maintenance of iPSCs and *LSR* knockdown**

622 Human iPSCs were maintained on matrigel (Corning) in mTesR1 medium (STEMCELL Technologies).
623 Cells were passaged approximately every 4-5 days. To passage iPSCs, they were washed with serum free
624 DMEM/F12 medium (STEMCELL Technologies) and incubated in DMEM/F12 with 1 mg/ml dispase
625 (Invitrogen) until cell edges started to detach from the dish. And then replaced with mTesR1. pipette
626 gently up and down to make the cells into small clumps and passaged onto fresh matrigel-coated plates.
627 For virus transfection experiments, above cells add full growth medium containing 1×10^7 MOI above
628 virus, the cells were incubated at 37°C for 12 h. Then, the medium was changed with fresh complete
629 medium and cultured for 48 h before harvesting for RNA isolation and organoid culture.

630 **Differentiation of iPSCs into human intestine organoid**

631 Differentiation of human iPSCs into organoid was run in accordance with the manufacturer's instructions

632 (STEMCELL Technologies). In brief, 1.5 × 10^5 iPSCs per ml were plated on matrigel coated tissue
633 culture plate (Thermo Fisher). Medium was changed to STEMdiff™ Endoderm Basal Medium
634 (STEMCELL Technologies) containing STEMdiff™ Definitive Endoderm Supplement CJ (STEMCELL
635 Technologies). On day 3, medium was changed to STEMdiff™. Endoderm Basal Medium containing
636 STEMdiff™. Gastrointestinal Supplement PK + STEMdiff™. Gastrointestinal Supplement UB
637 (STEMCELL Technologies). On day 4-9, medium was changed to Intestinal OGM (STEMCELL
638 Technologies) and incubate at 37°C with 5% CO2 and 95% humidity.

639 **Quantitative real time PCR**

640 The small intestine samples were homogenized in Trizol (Ambion, USA) to get total RNA. RNA was
641 reverse transcribed by using a reverse transcription system kit according to the instructions of the
642 manufacturer (Takara, Japan) followed by quantitative real time PCR (qRT-PCR) amplification using
643 SYBR Green PCR Master Mix (ABI, USA) and the Thermo Fisher QuantStudio3 system. The
644 Supplemental Table 2 contains the primer sequences used in this study. The expression levels of each
645 mRNA were calculated after normalizing to those of β-actin. Results were expressed as $2^{-\Delta Ct}$ values with
646 $\Delta CT = Ct_{gene} - Ct_{\beta\text{-actin}}$.

647 **Western blot analysis**

648 Total protein extracts were obtained by lysing isolated ISCs or small intestine tissues in RIPA lysis buffer
649 (Sangon Biotech) containing PMSF and phosphatase inhibitors (Sangon Biotech) on ice, supernatants
650 were collected after centrifugation at 4°C for 10 min at 12,000 × g. Then, the protein concentration was
651 assessed using a BCA protein assay (Takara). Proteins (50 μg) were separated in 10% SDS-PAGE and
652 then transferred onto PVDF membranes (0.22 μm), and then blocked with 5% skim milk dissolved in
653 TBST and incubated with the primary antibody at 4°C overnight. HRP-conjugated secondary antibodies
654 (Thermo Fisher) followed by ECL (Thermo Fisher) incubation allowed protein band detection. The
655 integration of all blots images was performed on Adobe Illustrator 2021. Image J v1.8.0 was used to
656 quantify western blotting results.

657 **Co-Immunoprecipitation (Co-IP)**

658 Isolated ISCs or HEK293 cells transfected with expressing vectors for LSR, YAP, and 14-3-3 zeta; LSR,
659 YAP, and 14-3-3 gamma; LSR, YAP, and PPP1CA; LSR, YAP, and PP2Ac; and YAP, 14-3-3 zeta and
660 PP2Ac were lysed in 50mM Tris (pH 8.0) by 25–30 repeated passages through a 25-gauge needle,
661 followed by centrifugation at 5,000 × g for 20 min, 4°C. The membranes of lysis were extracted using
662 CSK buffer (1% Triton X-100; 150 mM NaCl; 50 mM Tris, pH 8.0; and protease inhibitors). The
663 membrane extract was precleared by incubation with protein A/G-sepharose (invitrogen) prior to Co-IP.
664 The precleared membrane extract was incubated for 16 h at 4°C with anti-LSR, anti-YAP, anti-14-3-3
665 zeta, anti-14-3-3 gamma, anti-PPP1CA, anti-PP2Ac, anti-mouse IgG, or anti-Rabbit IgG antibodies.
666 Antibody-bound material was pelleted with protein A/G-sepharose, washed three times with CSK buffer,
667 and detected by immunoblotting.

668 **LC-MS/MS Analysis**

669 Follow the above Co-IP method, isolated ISCs and extracted the membranes of lysis. The precleared
670 membrane extract was incubated for 16 h at 4°C with anti-LSR and anti-mouse IgG (as negative control)
671 antibodies. Antibody-bound material was pelleted with protein A/G-sepharose, washed three times with
672 CSK buffer, and performing SDS-PAGE, and then cut the gel and detected.

673 The separated peptides were analyzed by Q Exactive HF-X mass spectrometer (Thermo Fisher) by
674 Novogene (China). The resulting spectra from each fraction were searched separately against uniprot
675 database by the search engines: Proteome Discoverer 2.2 (PD 2.2, Thermo). The search parameters are
676 set as follows: mass tolerance for precursor ion was 10 ppm and mass tolerance for product ion was 0.02
677 Da. Carbamidomethyl was specified in PD 2.2 as fixed modifications. Oxidation of methionine (M) and
678 acetylation of the N-terminus were specified in PD 2.2 as variable modifications. A maximum of 2 missed
679 cleavage sites were allowed. The identified protein contains at least 1 unique peptide with FDR no more
680 than 1%. Proteins containing similar peptides that could not be distinguished by MS/MS analysis were
681 identified as a same protein group.

682 **Data availability**

683 The raw RNA-seq data were deposited in NCBI sequence read archive (SRA) database, with the

accession number PRJNA769233. Additional details on protocols and databases/datasets used in this study are available from the corresponding authors on reasonable request.

Statistical analysis

The significance of differences between groups was tested by Prism 8 (GraphPad Software Inc.). Statistical analysis was performed using the unpaired *t* test to determine differences between two groups and ANOVA to compare data among groups. P-values less than 0.05 were interpreted as statistically significant. All data are presented as mean ± SEM and other details such as the number of replicates and the level of significance is mentioned in figure legends and supplementary information.

Acknowledgments

We thank Ping Li for animal husbandry. We thank the electron microscopic core lab of Shandong University for assistance on electron microscopy imaging. The work is funded by National Natural Science Foundation of China (81670620, 81870485, 81970578, and 81971281), Taishan Scholars Program of Shandong Province (ts20190953), Natural Science Foundation of Shandong Province (ZR2020QH066 and ZR2021QH115), Shandong First Medical University Academic Promotion Program (2020LI001), and Binzhou Medical University Independent Research Program.

Author contributions

Y. A., C. W., and B. F. designed and conducted *in vivo* and *in vitro* experiments, performed data analysis, and wrote the manuscript. Y. L., F. K., C. Z. and Z. C. performed histologic analysis. J. L., M. W. and H. S. performed mice genotyping. Y. G. and S. Z. designed and jointly supervised the study, analyzed the data, and wrote the manuscript.

Competing Interests statement

The authors declare no competing financial interests.

References

707 Adolph, T.E., M.F. Tomczak, L. Niederreiter, H.J. Ko, J. Bock, E. Martinez-Naves, J.N. Glickman, M.
708 Tschurtschenthaler, J. Hartwig, S. Hosomi, M.B. Flak, J.L. Cusick, K. Kohno, T. Iwawaki, S.
709 Billmann-Born, T. Raine, R. Bharti, R. Lucius, M.N. Kweon, S.J. Marciniak, A. Choi, S.J. Hagen,
710 S. Schreiber, P. Rosenstiel, A. Kaser, and R.S. Blumberg. 2013. Paneth cells as a site of
711 origin for intestinal inflammation. *Nature* 503:272-276.
712 Azzolin, L., T. Panciera, S. Soligo, E. Enzo, S. Bicciato, S. Dupont, S. Bresolin, C. Frasson, G. Basso, V.
713 Guzzardo, A. Fassina, M. Cordenonsi, and S. Piccolo. 2014. YAP/TAZ incorporation in the
714 beta-catenin destruction complex orchestrates the Wnt response. *Cell* 158:157-170.
715 Barry, E.R., T. Morikawa, B.L. Butler, K. Shrestha, R. de la Rosa, K.S. Yan, C.S. Fuchs, S.T. Magness, R.
716 Smits, S. Ogino, C.J. Kuo, and F.D. Camargo. 2013. Restriction of intestinal stem cell
717 expansion and the regenerative response by YAP. *Nature* 493:106-110.
718 Beyaz, S., M.D. Mana, J. Roper, D. Kedrin, A. Saadatpour, S.J. Hong, K.E. Bauer-Rowe, M.E. Xifaras,
719 A. Akkad, E. Arias, L. Pinello, Y. Katz, S. Shinagare, M. Abu-Remaileh, M.M. Mihaylova, D.W.
720 Lamming, R. Dogum, G. Guo, G.W. Bell, M. Selig, G.P. Nielsen, N. Gupta, C.R. Ferrone, V.
721 Deshpande, G.C. Yuan, S.H. Orkin, D.M. Sabatini, and O.H. Yilmaz. 2016. High-fat diet
722 enhances stemness and tumorigenicity of intestinal progenitors. *Nature* 531:53-58.
723 Bihain, B.E., and F.T. Yen. 1992. Free fatty acids activate a high-affinity saturable pathway for
724 degradation of low-density lipoproteins in fibroblasts from a subject homozygous for
725 familial hypercholesterolemia. *Biochemistry* 31:4628-4636.
726 Bjerknes, M., and H. Cheng. 1981. The stem-cell zone of the small intestinal epithelium. I. Evidence
727 from Paneth cells in the adult mouse. *The American journal of anatomy* 160:51-63.
728 Cai, J., N. Zhang, Y. Zheng, R.F. de Wilde, A. Maitra, and D. Pan. 2010. The Hippo signaling pathway
729 restricts the oncogenic potential of an intestinal regeneration program. *Genes &*
730 *development* 24:2383-2388.
731 Camargo, F.D., S. Gokhale, J.B. Johnnidis, D. Fu, G.W. Bell, R. Jaenisch, and T.R. Brummelkamp. 2007.
732 YAP1 increases organ size and expands undifferentiated progenitor cells. *Current biology :*
733 *CB* 17:2054-2060.
734 Chacon-Martinez, C.A., J. Koester, and S.A. Wickstrom. 2018. Signaling in the stem cell niche:
735 regulating cell fate, function and plasticity. *Development* 145:
736 Cheung, P., J. Xiol, M.T. Dill, W.C. Yuan, R. Panero, J. Roper, F.G. Osorio, D. Maglic, Q. Li, B. Gurung,
737 R.A. Calogero, O.H. Yilmaz, J. Mao, and F.D. Camargo. 2020. Regenerative
738 Reprogramming of the Intestinal Stem Cell State via Hippo Signaling Suppresses
739 Metastatic Colorectal Cancer. *Cell stem cell* 27:590-604 e599.
740 Coutinho, H.B., H.C. da Mota, V.B. Coutinho, T.I. Robalinho, A.F. Furtado, E. Walker, G. King, Y.R.
741 Mahida, H.F. Sewell, and D. Wakelin. 1998. Absence of lysozyme (muramidase) in the
742 intestinal Paneth cells of newborn infants with necrotising enterocolitis. *Journal of clinical*
743 *pathology* 51:512-514.
744 Dong, X., X.B. Zhang, P. Liu, Y. Tian, L. Li, and P. Gong. 2022. Lipolysis-Stimulated Lipoprotein
745 Receptor Impairs Hepatocellular Carcinoma and Inhibits the Oncogenic Activity of YAP1
746 via PPPY Motif. *Front Oncol* 12:
747 Dzulko, M., M. Pons, A. Henke, G. Schneider, and O.H. Kramer. 2020. The PP2A subunit PR130 is a
748 key regulator of cell development and oncogenic transformation. *Biochimica et*
749 *biophysica acta. Reviews on cancer* 1874:188453.
750 Fan, S., Y. Gao, A. Qu, Y. Jiang, H. Li, G. Xie, X. Yao, X. Yang, S. Zhu, T. Yagai, J. Tian, R. Wang, F.J.

751 Gonzalez, M. Huang, and H. Bi. 2022. YAP-TEAD mediates PPAR alpha-induced
752 hepatomegaly and liver regeneration in mice. *Hepatology* 75:74-88.
753 Frost, B.L., B.P. Modi, T. Jaksic, and M.S. Caplan. 2017. New Medical and Surgical Insights Into
754 Neonatal Necrotizing Enterocolitis: A Review. *JAMA pediatrics* 171:83-88.
755 Gjorevski, N., M. Nikolaev, T.E. Brown, O. Mitrofanova, N. Brandenberg, F.W. DelRio, F.M. Yavitt, P.
756 Liberali, K.S. Anseth, and M.P. Lutolf. 2022. Tissue geometry drives deterministic organoid
757 patterning. *Science* 375:eaaw9021.
758 Gjorevski, N., N. Sachs, A. Manfrin, S. Giger, M.E. Bragina, P. Ordonez-Moran, H. Clevers, and M.P.
759 Lutolf. 2016. Designer matrices for intestinal stem cell and organoid culture. *Nature*
760 539:560-564.
761 Goga, A., B. Yagabasan, K. Herrmanns, S. Godbersen, P.N. Silva, R. Denzler, M. Zund, M. Furter, G.
762 Schwank, S. Sunagawa, W.D. Hardt, and M. Stoffel. 2021. miR-802 regulates Paneth cell
763 function and enterocyte differentiation in the mouse small intestine. *Nature*
764 *communications* 12:3339.
765 Gomez-Suarez, M., I.Z. Gutierrez-Martinez, J.A. Hernandez-Trejo, M. Hernandez-Ruiz, D. Suarez-
766 Perez, A. Candelario, R. Kamekura, O. Medina-Contreras, M. Schnoor, V. Ortiz-Navarrete,
767 N. Villegas-Sepulveda, C. Parkos, A. Nusrat, and P. Nava. 2016. 14-3-3 Proteins regulate
768 Akt Thr308 phosphorylation in intestinal epithelial cells. *Cell Death Differ* 23:1060-1072.
769 Gong, Y., M. Yu, J. Yang, E. Gonzales, R. Perez, M. Hou, P. Tripathi, K.S. Hering-Smith, L.L. Hamm,
770 and J. Hou. 2014. The Cap1-claudin-4 regulatory pathway is important for renal chloride
771 reabsorption and blood pressure regulation. *Proceedings of the National Academy of*
772 *Sciences of the United States of America* 111:E3766-3774.
773 Gregorieff, A., Y. Liu, M.R. Inanlou, Y. Khomchuk, and J.L. Wrana. 2015. Yap-dependent
774 reprogramming of Lgr5(+) stem cells drives intestinal regeneration and cancer. *Nature*
775 526:715-718.
776 Guillermin, O., N. Angelis, C.M. Sidor, R. Ridgway, A. Baulies, A. Kucharska, P. Antas, M.R. Rose, J.
777 Cordero, O. Sansom, V.S.W. Li, and B.J. Thompson. 2021. Wnt and Src signals converge
778 on YAP-TEAD to drive intestinal regeneration. *The EMBO journal* 40:e105770.
779 Hayashi, S., and A.P. McMahon. 2002. Efficient recombination in diverse tissues by a tamoxifen-
780 inducible form of Cre: a tool for temporally regulated gene activation/inactivation in the
781 mouse. *Developmental biology* 244:305-318.
782 Hemmasi, S., B.A. Czulkies, B. Schorch, A. Veit, K. Aktories, and P. Papatheodorou. 2015. Interaction
783 of the Clostridium difficile Binary Toxin CDT and Its Host Cell Receptor, Lipolysis-
784 stimulated Lipoprotein Receptor (LSR). *The Journal of biological chemistry* 290:14031-
785 14044.
786 Hu, J.K., W. Du, S.J. Shelton, M.C. Oldham, C.M. DiPersio, and O.D. Klein. 2017. An FAK-YAP-mTOR
787 Signaling Axis Regulates Stem Cell-Based Tissue Renewal in Mice. *Cell stem cell* 21:91-
788 106 e106.
789 Kang, J.X., J.B. Wan, and C. He. 2014. Concise review: Regulation of stem cell proliferation and
790 differentiation by essential fatty acids and their metabolites. *Stem Cells* 32:1092-1098.
791 Konno, T., T. Kohno, S. Kikuchi, H. Shimada, S. Satohisa, T. Saito, M. Kondoh, and T. Kojima. 2020.
792 Epithelial barrier dysfunction and cell migration induction via JNK/cofilin/actin by
793 angubindin-1. *Tissue barriers* 8:1695475.
794 Koo, J.H., and K.L. Guan. 2018. Interplay between YAP/TAZ and Metabolism. *Cell metabolism*

28:196-206.
Lapi, E., S. Di Agostino, S. Donzelli, H. Gal, E. Domany, G. Rechavi, P.P. Pandolfi, D. Givol, S. Strano, X. Lu, and G. Blandino. 2008. PML, YAP, and p73 are components of a proapoptotic autoregulatory feedback loop. *Molecular cell* 32:803-814.
Li, Q., Y. Sun, G.K. Jarugumilli, S. Liu, K. Dang, J.L. Cotton, J. Xiol, P.Y. Chan, M. DeRan, L. Ma, R. Li, L.J. Zhu, J.H. Li, A.B. Leiter, Y.T. Ip, F.D. Camargo, X. Luo, R.L. Johnson, X. Wu, and J. Mao. 2020. Lats1/2 Sustain Intestinal Stem Cells and Wnt Activation through TEAD-Dependent and Independent Transcription. *Cell stem cell* 26:675-692 e678.
Li, V.S.W. 2019. Yap in regeneration and symmetry breaking. *Nature cell biology* 21:665-667.
Lueschow, S.R., and S.J. McElroy. 2020. The Paneth Cell: The Curator and Defender of the Immature Small Intestine. *Frontiers in immunology* 11:587.
Lueschow, S.R., J. Stumphy, H. Gong, S.L. Kern, T.G. Elgin, M.A. Underwood, K.M. Kalanetra, D.A. Mills, M.H. Wong, D.K. Meyerholz, M. Good, and S.J. McElroy. 2018. Loss of murine Paneth cell function alters the immature intestinal microbiome and mimics changes seen in neonatal necrotizing enterocolitis. *PloS one* 13:e0204967.
Lukonin, I., D. Serra, L. Challet Meylan, K. Volkmann, J. Baaten, R. Zhao, S. Meeusen, K. Colman, F. Maurer, M.B. Stadler, J. Jenkins, and P. Liberali. 2020. Phenotypic landscape of intestinal organoid regeneration. *Nature* 586:275-280.
Madison, B.B., L. Dunbar, X.T. Qiao, K. Braunstein, E. Braunstein, and D.L. Gumucio. 2002. Cis elements of the villin gene control expression in restricted domains of the vertical (crypt) and horizontal (duodenum, cecum) axes of the intestine. *The Journal of biological chemistry* 277:33275-33283.
Maehama, T., M. Nishio, J. Otani, T.W. Mak, and A. Suzuki. 2021. The role of Hippo-YAP signaling in squamous cell carcinomas. *Cancer science* 112:51-60.
Mann, C.J., J. Khallou, O. Chevreuil, A.A. Troussard, L.M. Guermani, K. Launay, B. Delplanque, F.T. Yen, and B.E. Bihain. 1995. Mechanism of activation and functional significance of the lipolysis-stimulated receptor. Evidence for a role as chylomicron remnant receptor. *Biochemistry* 34:10421-10431.
Masuda, S., Y. Oda, H. Sasaki, J. Ikenouchi, T. Higashi, M. Akashi, E. Nishi, and M. Furuse. 2011. LSR defines cell corners for tricellular tight junction formation in epithelial cells. *Journal of cell science* 124:548-555.
Meng, Z., T. Moroishi, and K.L. Guan. 2016. Mechanisms of Hippo pathway regulation. *Genes & development* 30:1-17.
Mesli, S., S. Javorschi, A.M. Berard, M. Landry, H. Priddle, D. Kivlichan, A.J. Smith, F.T. Yen, B.E. Bihain, and M. Darmon. 2004. Distribution of the lipolysis stimulated receptor in adult and embryonic murine tissues and lethality of LSR-/- embryos at 12.5 to 14.5 days of gestation. *European journal of biochemistry* 271:3103-3114.
MohanKumar, K., N. Kaza, R. Jagadeeswaran, S.A. Garzon, A. Bansal, A.R. Kurundkar, K. Namachivayam, J.I. Remon, C.R. Bandepalli, X. Feng, J.H. Weitkamp, and A. Maheshwari. 2012. Gut mucosal injury in neonates is marked by macrophage infiltration in contrast to pleomorphic infiltrates in adult: evidence from an animal model. *American journal of physiology. Gastrointestinal and liver physiology* 303:G93-102.
Namachivayam, K., K. MohanKumar, D.R. Shores, S.K. Jain, J. Fundora, A.D. Everett, L. He, H. Pan, S.A. Wickline, and A. Maheshwari. 2020. Targeted inhibition of thrombin attenuates

839 murine neonatal necrotizing enterocolitis. *Proceedings of the National Academy of*
840 *Sciences of the United States of America* 117:10958-10969.
841 Narvekar, P., M. Berriel Diaz, A. Krones-Herzig, U. Hardeland, D. Strzoda, S. Stohr, M. Frohme, and
842 S. Herzig. 2009. Liver-specific loss of lipolysis-stimulated lipoprotein receptor triggers
843 systemic hyperlipidemia in mice. *Diabetes* 58:1040-1049.
844 Oh, H., and K.D. Irvine. 2009. In vivo analysis of Yorkie phosphorylation sites. *Oncogene* 28:1916-
845 1927.
846 Papatheodorou, P., J.E. Carette, G.W. Bell, C. Schwan, G. Guttenberg, T.R. Brummelkamp, and K.
847 Aktories. 2011. Lipolysis-stimulated lipoprotein receptor (LSR) is the host receptor for the
848 binary toxin Clostridium difficile transferase (CDT). *Proceedings of the National Academy*
849 *of Sciences of the United States of America* 108:16422-16427.
850 Paroni, G., N. Cernotta, C. Dello Russo, P. Gallinari, M. Pallaoro, C. Foti, F. Talamo, L. Orsatti, C.
851 Steinkuhler, and C. Brancolini. 2008. PP2A regulates HDAC4 nuclear import. *Molecular*
852 *biology of the cell* 19:655-667.
853 Polyak, S., A. Mach, S. Porvasnik, L. Dixon, T. Conlon, K.E. Erger, A. Acosta, A.J. Wright, M. Campbell-
854 Thompson, I. Zolotukhin, C. Wasserfall, and C. Mah. 2012. Identification of adeno-
855 associated viral vectors suitable for intestinal gene delivery and modulation of
856 experimental colitis. *American journal of physiology. Gastrointestinal and liver physiology*
857 302:G296-308.
858 Poon, K., S. Mandava, K. Chen, J.R. Barson, S. Buschlen, and S.F. Leibowitz. 2013. Prenatal Exposure
859 to Dietary Fat Induces Changes in the Transcriptional Factors, TEF and YAP, Which May
860 Stimulate Differentiation of Peptide Neurons in Rat Hypothalamus. *Plos One* 8:
861 Qi, Q., D.Y. Li, H.R. Luo, K.L. Guan, and K. Ye. 2015. Netrin-1 exerts oncogenic activities through
862 enhancing Yes-associated protein stability. *Proceedings of the National Academy of*
863 *Sciences of the United States of America* 112:7255-7260.
864 Reaves, D.K., K.A. Hoadley, K.D. Fagan-Solis, D.D. Jima, M. Bereman, L. Thorpe, J. Hicks, D.
865 McDonald, M.A. Troester, C.M. Perou, and J.M. Fleming. 2017. Nuclear Localized LSR: A
866 Novel Regulator of Breast Cancer Behavior and Tumorigenesis. *Mol Cancer Res* 15:165-
867 178.
868 Resnik-Docampo, M., C.L. Koehler, R.I. Clark, J.M. Schinaman, V. Sauer, D.M. Wong, S. Lewis, C.
869 D'Alterio, D.W. Walker, and D.L. Jones. 2017. Tricellular junctions regulate intestinal stem
870 cell behaviour to maintain homeostasis. *Nature cell biology* 19:52-59.
871 Santinon, G., A. Pocaterra, and S. Dupont. 2016. Control of YAP/TAZ Activity by Metabolic and
872 Nutrient-Sensing Pathways. *Trends in cell biology* 26:289-299.
873 Sato, T., R.G. Vries, H.J. Snippert, M. van de Wetering, N. Barker, D.E. Stange, J.H. van Es, A. Abo, P.
874 Kujala, P.J. Peters, and H. Clevers. 2009. Single Lgr5 stem cells build crypt-villus structures
875 in vitro without a mesenchymal niche. *Nature* 459:262-265.
876 Schlegelmilch, K., M. Mohseni, O. Kirak, J. Pruszak, J.R. Rodriguez, D. Zhou, B.T. Kreger, V.
877 Vasioukhin, J. Avruch, T.R. Brummelkamp, and F.D. Camargo. 2011. Yap1 acts downstream
878 of alpha-catenin to control epidermal proliferation. *Cell* 144:782-795.
879 Serra, D., U. Mayr, A. Boni, I. Lukonin, M. Rempfler, L. Challet Meylan, M.B. Stadler, P. Strnad, P.
880 Papasaikas, D. Vischi, A. Waldt, G. Roma, and P. Liberali. 2019. Self-organization and
881 symmetry breaking in intestinal organoid development. *Nature* 569:66-72.
882 Shimada, H., S. Abe, T. Kohno, S. Satohisa, T. Konno, S. Takahashi, T. Hatakeyama, C. Arimoto, T.

Kakuki, Y. Kaneko, K.I. Takano, T. Saito, and T. Kojima. 2017. Loss of tricellular tight junction protein LSR promotes cell invasion and migration via upregulation of TEAD1/AREG in human endometrial cancer. *Sci Rep* 7:37049.

Sohet, F., C. Lin, R.N. Munji, S.Y. Lee, N. Ruderisch, A. Soung, T.D. Arnold, N. Derugin, Z.S. Vexler, F.T. Yen, and R. Daneman. 2015. LSR/angulin-1 is a tricellular tight junction protein involved in blood-brain barrier formation. *The Journal of cell biology* 208:703-711.

Stevers, L.M., E. Sijbesma, M. Botta, C. MacKintosh, T. Obsil, I. Landrieu, Y. Cau, A.J. Wilson, A. Karawajczyk, J. Eickhoff, J. Davis, M. Hann, G. O'Mahony, R.G. Doveston, L. Brunsveld, and C. Ottmann. 2018. Modulators of 14-3-3 Protein-Protein Interactions. *Journal of medicinal chemistry* 61:3755-3778.

Sugawara, T., K. Furuse, T. Otani, T. Wakayama, and M. Furuse. 2021. Angulin-1 seals tricellular contacts independently of tricellulin and claudins. *The Journal of cell biology* 220:

Sukhotnik, I., L. Hayari, Y. Bashenko, E. Chemodanov, J. Mogilner, R. Shamir, F. Bar Yosef, R. Shaoul, and A.G. Coran. 2008. Dietary palmitic acid modulates intestinal re-growth after massive small bowel resection in a rat. *Pediatric surgery international* 24:1313-1321.

Sun, B., F.J. Zhong, C. Xu, Y.M. Li, Y.R. Zhao, M.M. Cao, and L.Y. Yang. 2021. Programmed cell death 10 promotes metastasis and epithelial-mesenchymal transition of hepatocellular carcinoma via PP2Ac-mediated YAP activation. *Cell death & disease* 12:849.

Takahashi, Y., S. Serada, T. Ohkawara, M. Fujimoto, K. Hiramatsu, Y. Ueda, T. Kimura, H. Takemori, and T. Naka. 2021. LSR promotes epithelial ovarian cancer cell survival under energy stress through the LKB1-AMPK pathway. *Biochem Bioph Res Co* 537:93-99.

Totaro, A., T. Panciera, and S. Piccolo. 2018. YAP/TAZ upstream signals and downstream responses. *Nature cell biology* 20:888-899.

Underwood, M.A. 2012. Paneth cells and necrotizing enterocolitis. *Gut microbes* 3:562-565.

Wang, L., S. Wang, Y. Shi, R. Li, S. Gunther, Y.T. Ong, M. Potente, Z. Yuan, E. Liu, and S. Offermanns. 2020a. YAP and TAZ protect against white adipocyte cell death during obesity. *Nat Commun* 11:5455.

Wang, L., S.P. Wang, Y. Shi, R. Li, S. Gunther, Y.T. Ong, M. Potente, Z.Y. Yuan, E.Q. Liu, and S. Offermanns. 2020b. YAP and TAZ protect against white adipocyte cell death during obesity. *Nat Commun* 11:

Wehkamp, J., and E.F. Stange. 2020. An Update Review on the Paneth Cell as Key to Ileal Crohn's Disease. *Frontiers in immunology* 11:646.

Weis, V.G., A.C. Deal, G. Mekkey, C. Clouse, M. Gaffley, E. Whitaker, C.B. Peeler, J.A. Weis, M.Z. Schwartz, and A. Atala. 2021. Human placental-derived stem cell therapy ameliorates experimental necrotizing enterocolitis. *American journal of physiology. Gastrointestinal and liver physiology* 320:G658-G674.

Xi, P., L. Zhou, M. Wang, J.P. Liu, and Y.S. Cong. 2013. Serine/threonine-protein phosphatase 2A physically interacts with human telomerase reverse transcriptase hTERT and regulates its subcellular distribution. *Journal of cellular biochemistry* 114:409-417.

Yan, H., C.C. Yu, S.A. Fine, A.L. Youssof, Y.R. Yang, J. Yan, D.C. Karg, E.C. Cheung, R.A. Friedman, H. Ying, E.I. Chen, J. Luo, Y. Miao, W. Qiu, and G.H. Su. 2021. Loss of the wild-type KRAS allele promotes pancreatic cancer progression through functional activation of YAP1. *Oncogene* 40:6759-6771.

Yen, F.T., C.J. Mann, L.M. Guermani, N.F. Hannouche, N. Hubert, C.A. Hornick, V.N. Bordeau, G.

927 Agnani, and B.E. Bihain. 1994. Identification of a lipolysis-stimulated receptor that is
928 distinct from the LDL receptor and the LDL receptor-related protein. *Biochemistry*
929 33:1172-1180.
930 Yen, F.T., M. Masson, N. Clossais-Besnard, P. Andre, J.M. Grosset, L. Bougueleret, J.B. Dumas, O.
931 Guerassimenko, and B.E. Bihain. 1999. Molecular cloning of a lipolysis-stimulated remnant
932 receptor expressed in the liver. *The Journal of biological chemistry* 274:13390-13398.
933 Yuan, L., Y. Mao, W. Luo, W. Wu, H. Xu, X.L. Wang, and Y.H. Shen. 2017. Palmitic acid dysregulates
934 the Hippo-YAP pathway and inhibits angiogenesis by inducing mitochondrial damage
935 and activating the cytosolic DNA sensor cGAS-STING-IRF3 signaling mechanism. *J Biol*
936 *Chem* 292:15002-15015.
937 Zhao, B., L. Li, K. Tumaneng, C.Y. Wang, and K.L. Guan. 2010. A coordinated phosphorylation by
938 Lats and CK1 regulates YAP stability through SCF(beta-TRCP). *Genes & development*
939 24:72-85.
940 Zhou, D., Y. Zhang, H. Wu, E. Barry, Y. Yin, E. Lawrence, D. Dawson, J.E. Willis, S.D. Markowitz, F.D.
941 Camargo, and J. Avruch. 2011. Mst1 and Mst2 protein kinases restrain intestinal stem cell
942 proliferation and colonic tumorigenesis by inhibition of Yes-associated protein (Yap)
943 overabundance. *Proceedings of the National Academy of Sciences of the United States of*
944 *America* 108:E1312-1320.
945 Zolnierowicz, S. 2000. Type 2A protein phosphatase, the complex regulator of numerous signaling
946 pathways. *Biochemical pharmacology* 60:1225-1235.

947

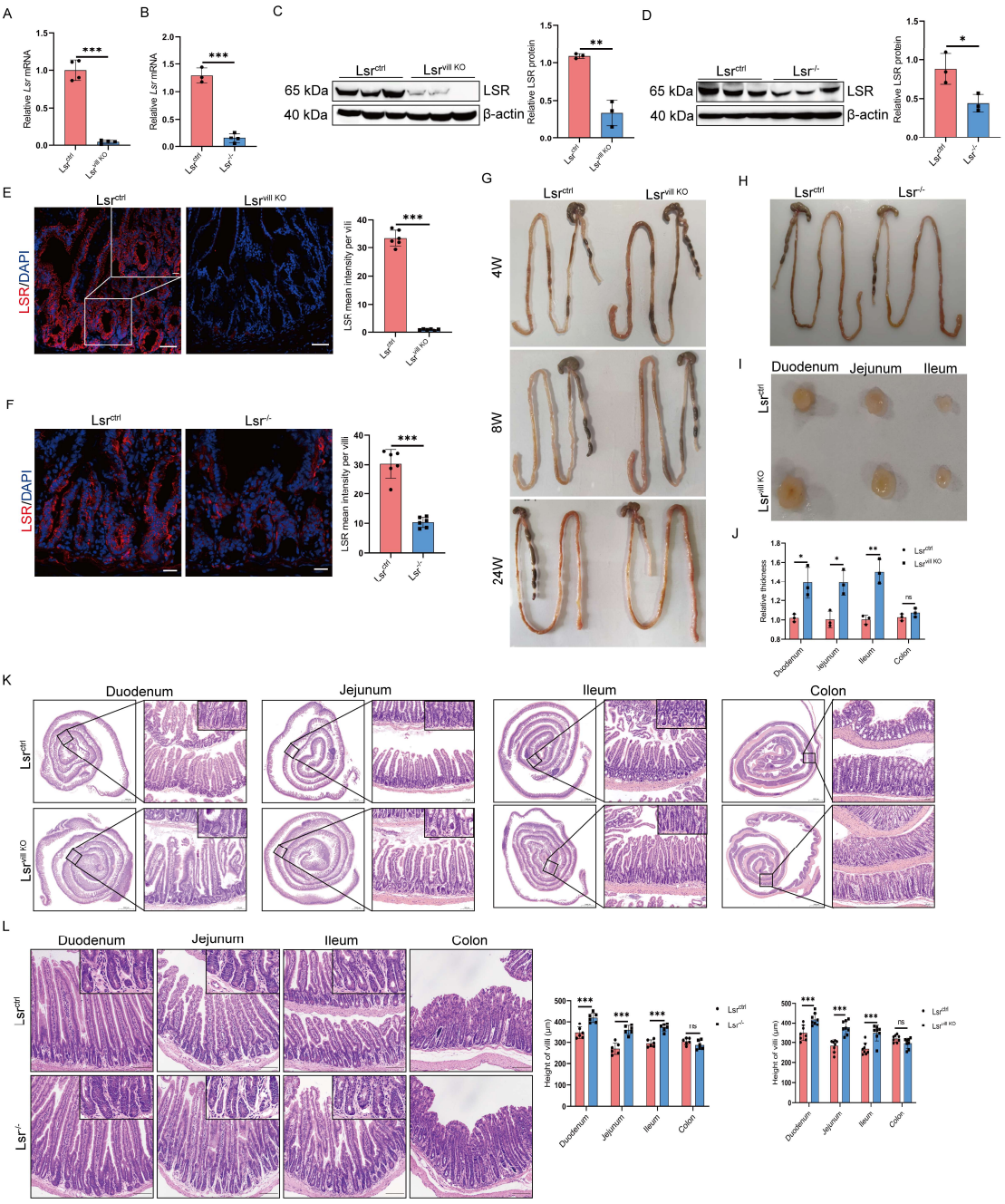

Fig. 1. Generation and characterization of conditional Lsr knockout mice.

(A and B) Expression of *Lsr* mRNA assessed by qRT–PCR in small intestines from Lsr^{ctrl} and $Lsr^{vill\ KO}$ mice (A) and Lsr^{ctrl} and $Lsr^{-/-}$ mice (B) (n=4). (C and D) Western blot and quantification analysis of LSR in small intestines from Lsr^{ctrl} and $Lsr^{vill\ KO}$ mice (C) and Lsr^{ctrl} and $Lsr^{-/-}$ mice (D) (n=3). (E and F) LSR immunofluorescence and quantification analysis of small intestines from Lsr^{ctrl} and $Lsr^{vill\ KO}$ mice (E) and Lsr^{ctrl} and $Lsr^{-/-}$ mice (F) (n=6). (G) Longitudinal views of intestine from Lsr^{ctrl} and $Lsr^{vill\ KO}$ mice at 4, 8 and 24 weeks of age. (H) Longitudinal views of intestine from Lsr^{ctrl} and $Lsr^{-/-}$ mice. (I) Transverse views of intestine from Lsr^{ctrl} and $Lsr^{vill\ KO}$ littermate mice. (J) Analysis of intestinal wall thickness of

957 Lsr^{ctrl} and $Lsr^{vill\ KO}$ mice (n=3). (K) Representative H&E-stained transverse segments and quantification
958 analysis of Lsr^{ctrl} and $Lsr^{vill\ KO}$ mouse intestines (n=6). (L) Representative H&E-stained small intestine
959 and quantification analysis of Lsr^{ctrl} and $Lsr^{-/-}$ mice (n=6). Scale bars: E, 50 μm; F, 20 μm; K and J, 100
960 μm. *$P < 0.05$, **$P < 0.01$, ***$P < 0.001$.*
961

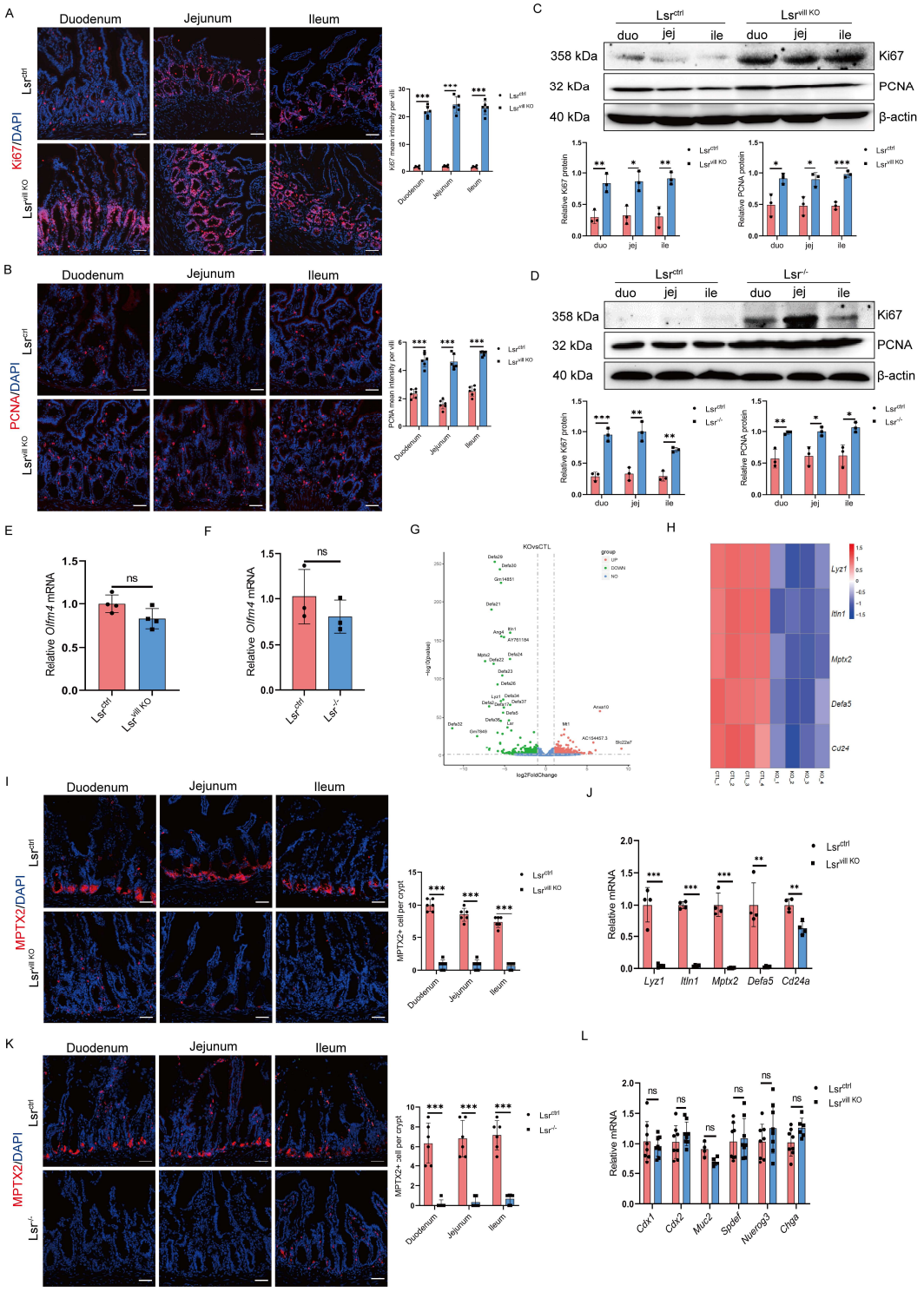

Fig. 2. LSR ablation results in increased numbers of proliferating cells and loss of Paneth cell lineage in the small intestine.

(A and B) Ki67 (A) and PCNA (B) immunofluorescence and quantification analysis in duodenal, jejunal and ileal segments from Lsr^{ctrl} and $Lsr^{vill\ KO}$ mice (n=6). (C and D) Western blot and quantification analysis of Ki67 and PCNA protein expression in duodenal, jejunal and ileal segments from Lsr^{ctrl} and

968 $Lsr^{vill\ KO}$ mice (C) and Lsr^{ctrl} and $Lsr^{-/-}$ mice (D) (n=3). (E and F) Expression of *Olfm4* mRNA assessed
969 by qRT–PCR in small intestines from Lsr^{ctrl} and $Lsr^{vill\ KO}$ mice (E) and Lsr^{ctrl} and $Lsr^{-/-}$ mice (F) (n=4).
970 (G) Differentially expressed genes ($Lsr^{vill\ KO}$ vs. Lsr^{ctrl}) are shown on a volcano plot (n=4; fold change >
971 2, $P < 0.05$). (H) Heatmap showing unsupervised hierarchical clustering of Paneth cell-related genes. (I)
972 MPTX2 immunofluorescence and quantification analysis in duodenal, jejunal and ileal segments from
973 Lsr^{ctrl} and $Lsr^{vill\ KO}$ mice (n=6). (J) qRT-PCR validating several downregulated Paneth cell markers in
974 small intestines from Lsr^{ctrl} and $Lsr^{vill\ KO}$ mice (n=4). (K) MPTX2 immunofluorescence and quantification
975 analysis in duodenal, jejunal and ileal segments from Lsr^{ctrl} and $Lsr^{-/-}$ mice (n=6). (L) qRT–PCR analysis
976 of the mRNA expression of columnar absorptive cell markers (*Cdx1* and *Cdx2*), goblet cell markers
977 (*Muc2* and *Spdef*), and enteroendocrine cell markers (*Neurog3* and *Chga*) in small intestines from Lsr^{ctrl}
978 and $Lsr^{vill\ KO}$ mice (n=8). Scale bars: A, B, I and K, 50 μm. $^{*}P < 0.05$, $^{**}P < 0.01$, $^{***}P < 0.001$.
979

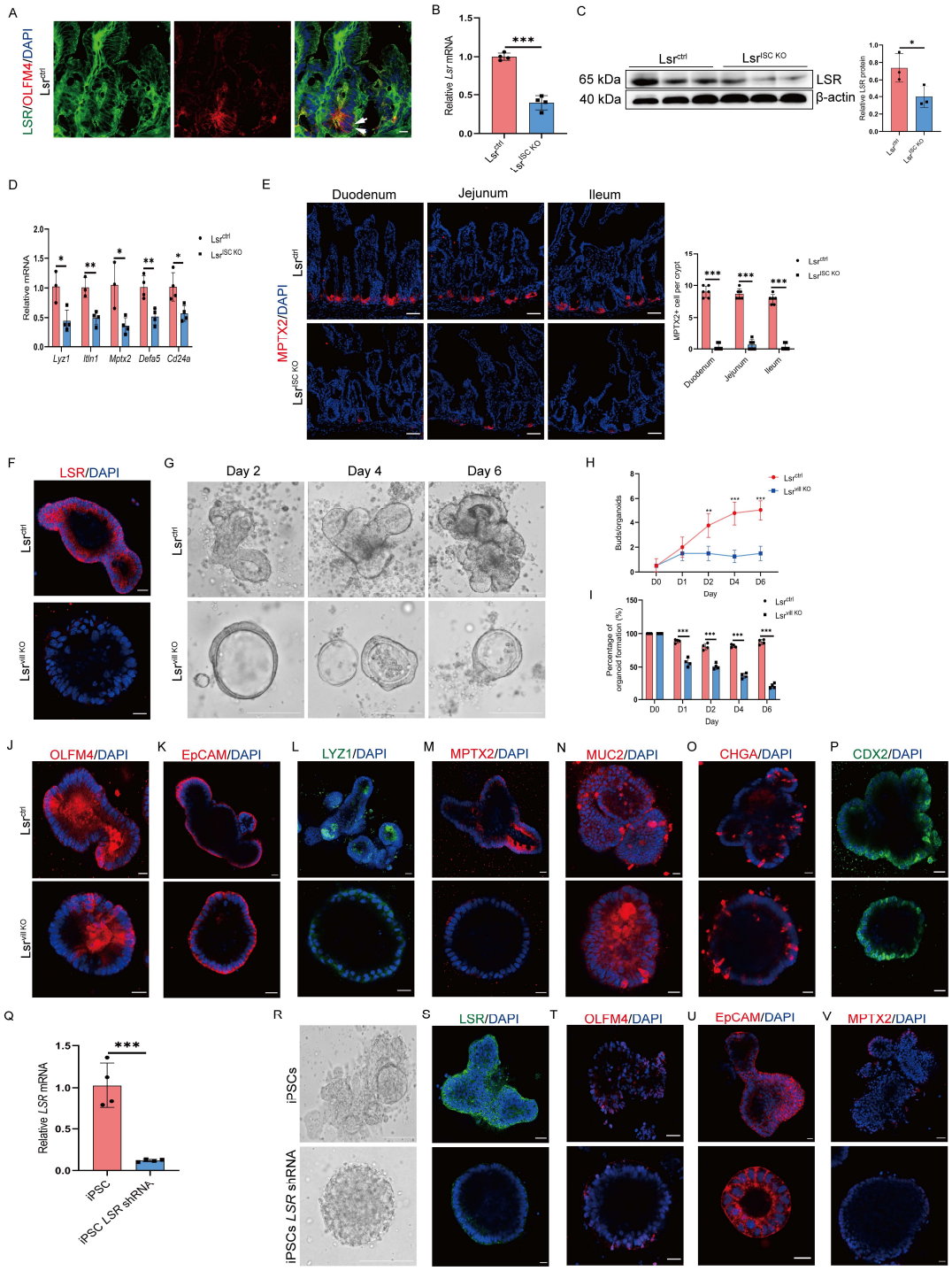

Fig. 3. LSR is required for Lgr5^{+} ISCs to Paneth cell differentiation.

(A) LSR and OLFM4 immunofluorescence in small intestines from Lsr^{ctrl} mice (arrows indicated colocalization of LSR and OLFM4 in ISCs). (B) Expression of *Lsr* mRNA assessed by qRT–PCR in small intestines from Lsr^{ctrl} and Lsr$^{ISC\ KO}$ mice (n=4). (C) Western blot and quantification analysis of LSR in small intestines from Lsr^{ctrl} and Lsr$^{ISC\ KO}$ mice (n=3). (D) Expression of Paneth cell markers (*Lyz1, Itln1, Mptx2, Defa5* and *Cd24a*) mRNA assessed by qRT–PCR in small intestines from Lsr^{ctrl} and Lsr^{ISC}

^{KO} mice (n=4). (E) MPTX2 immunofluorescence and quantification analysis in duodenal, jejunal and ileal segments from Lsr^{ctrl} and $Lsr^{ISC\ KO}$ mice (n=6). (F and G) LSR immunofluorescence (F) and bright field images (G) of organoids established from intestinal crypts of Lsr^{ctrl} and $Lsr^{vill\ KO}$ mice. (H and I) Quantification of the average number of buds per organoid (H) and percentage of organoid formation per well (n=3 wells per group) (I). (J-P) OLFM4 (J), EpCAM (K), LYZ1 (L), MPTX2 (M), MUC2 (N), CHGA (O) and CDX2 (P) immunofluorescence of organoids established from intestinal crypts of Lsr^{ctrl} and $Lsr^{vill\ KO}$ mice. (Q) Expression of *LSR* mRNA assessed by qRT–PCR in control and *LSR* knockdown human iPSCs (n=3). (R-V) Bright field images (R) and LSR (S) OLFM4 (T), EpCAM (U) and MPTX2 (V) immunofluorescence of organoids differentiated from control and *LSR* knockdown human iPSCs. Scale bars: A, 10μm; E, S, T and V, 50 μm; F, J, K, L, M, N, O, P and U, 20 μm; G and R, 125 μm. $*P < 0.05$, $**P < 0.01$, $***P < 0.001$.

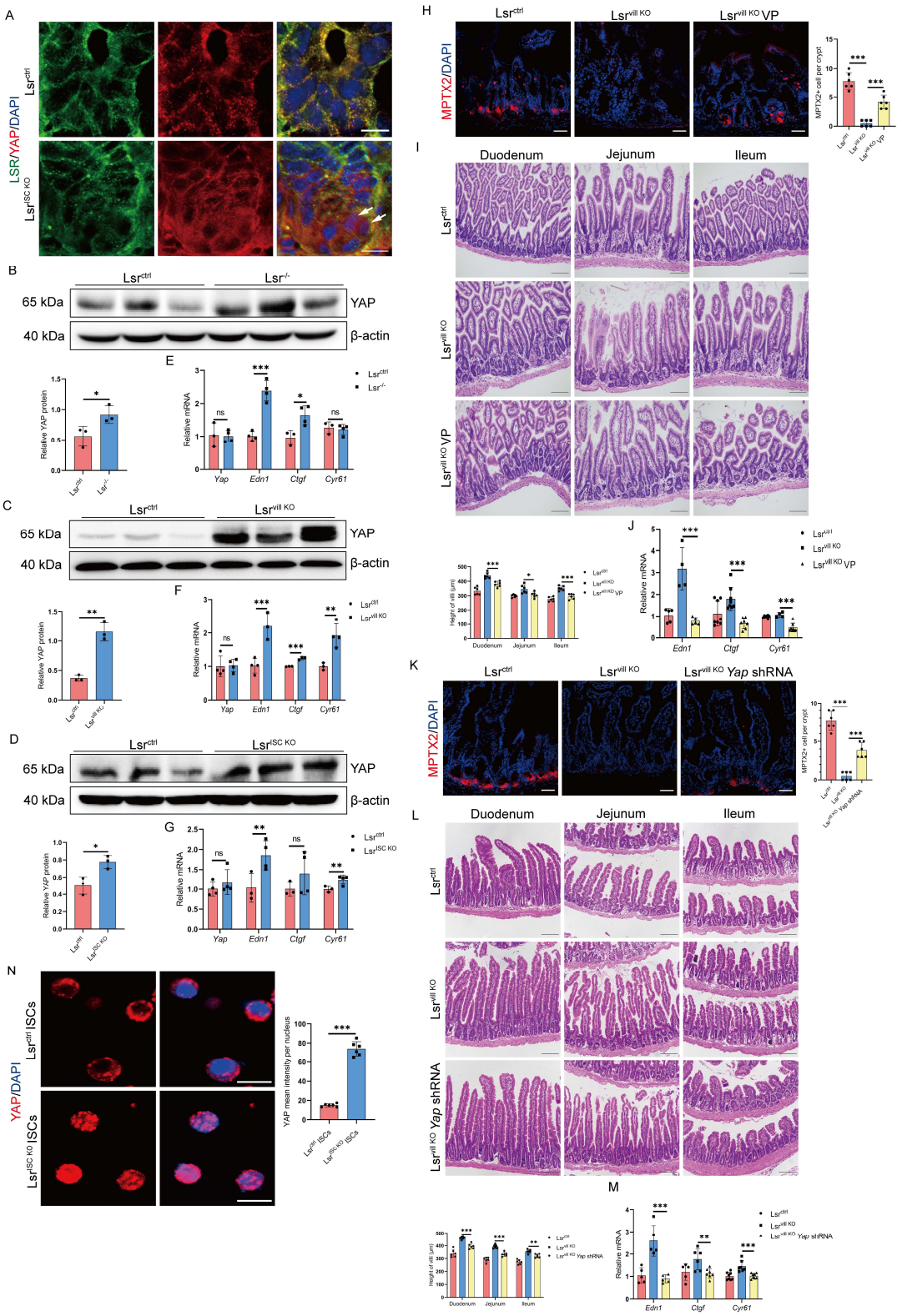

Fig. 4. Loss of LSR results in upregulation and activation of YAP.

(A) LSR and YAP immunofluorescence in small intestines from Lsr^{ctrl} and $Lsr^{ISC\ KO}$ mice (arrows indicated the ISCs). (B-D) Western blot and quantification analysis for YAP of small intestine lysates from Lsr^{ctrl} and $Lsr^{-/-}$ mice (B), Lsr^{ctrl} and $Lsr^{vill\ KO}$ mice (C) and Lsr^{ctrl} and $Lsr^{ISC\ KO}$ mice (D) (n=3). (E-

1004 G) Expression of *Yap, Edn1, Ctgf,* and *Cyr61* mRNA assessed by qRT–PCR in small intestines from
1005 Lsr^{ctrl} and $Lsr^{-/-}$ mice (E), Lsr^{ctrl} and $Lsr^{vill\ KO}$ mice (F) and Lsr^{ctrl} and $Lsr^{ISC\ KO}$ mice (G) (n=4). (H) MPTX2
1006 immunofluorescence and quantification analysis in small intestines from Lsr^{ctrl} mice, $Lsr^{vill\ KO}$ mice, and
1007 $Lsr^{vill\ KO}$ mice treated with VP (n=6). (I) H&E staining and quantification analysis in small intestine from
1008 Lsr^{ctrl} mice, $Lsr^{vill\ KO}$ mice, and $Lsr^{vill\ KO}$ mice treated with VP (n=6). (J) qRT-PCR analysis for YAP targets
1009 in small intestine from Lsr^{ctrl} mice, $Lsr^{vill\ KO}$ mice, and $Lsr^{vill\ KO}$ mice treated with VP (n=4). (K) MPTX2
1010 immunofluorescence and quantification analysis in small intestines from Lsr^{ctrl} mice, $Lsr^{vill\ KO}$ mice, and
1011 $Lsr^{vill\ KO}$ mice transduced with lentivirus expressing *Yap* shRNA (n=6). (L) H&E staining and
1012 quantification analysis in small intestine from Lsr^{ctrl} mice, $Lsr^{vill\ KO}$ mice, and $Lsr^{vill\ KO}$ mice treated with
1013 lentivirus expressing *Yap* shRNA (n=6). (M) qRT–PCR analysis for YAP targets in small intestine from
1014 Lsr^{ctrl} mice, $Lsr^{vill\ KO}$ mice, and $Lsr^{vill\ KO}$ mice treated with lentivirus expressing *Yap* shRNA (n=4). (N)
1015 YAP immunofluorescence and quantification analysis in ISCs isolated from Lsr^{ctrl} and $Lsr^{ISC\ KO}$ mice
1016 (n=6). Scale bars: A and N, 10 μm; H and K, 50 μm; I and L, 100 μm. $^{*}P < 0.05$, $^{**}P < 0.01$, $^{***}P <$
1017 0.001.
1018

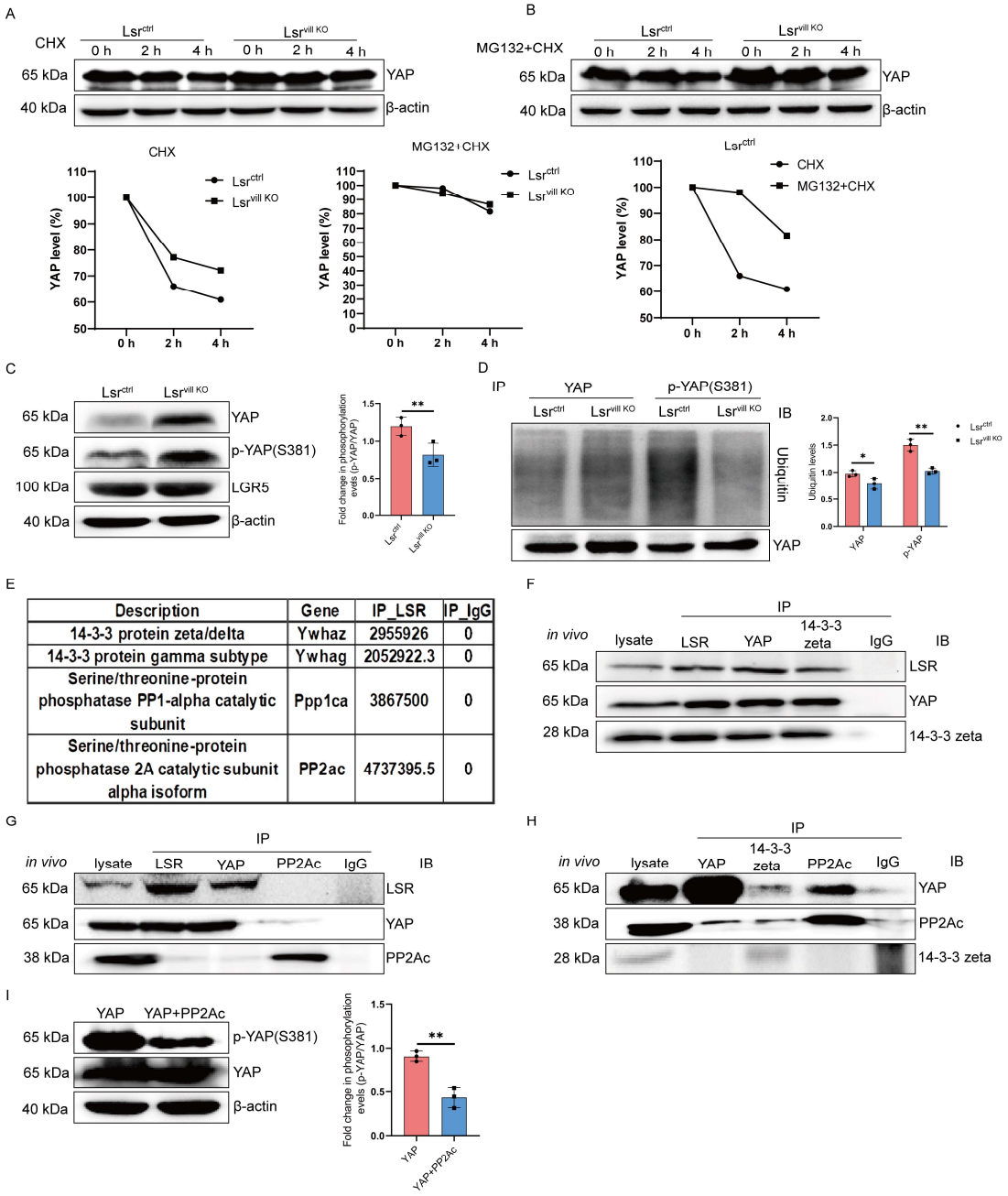

Description	Gene	IP_LSR	IP_IgG
14-3-3 protein zeta/delta	Ywhaz	2955926	0
14-3-3 protein gamma subtype	Ywhag	2052922.3	0
Serine/threonine-protein phosphatase PP1-alpha catalytic subunit	Ppp1ca	3867500	0
Serine/threonine-protein phosphatase 2A catalytic subunit alpha isoform	PP2ac	4737395.5	0

Fig. 5. 14-3-3 zeta and PP2Ac are involved in the regulation of YAP by LSR.

(A and B) Western blot analysis for YAP in isolated ISCs treated with 5 mg/ml CHX for 0-4 h (A) or pretreated with 10 mM MG132 for 2 h and then treated with 5 mg/ml CHX for 0-4 h (B). And line graph showing the relative YAP protein levels quantified by YAP/β-actin ratio, which was arbitrarily set to 100% at the 0 hour point. (C) Western blot and quantification analysis for YAP, p-YAP (Ser381), LGR5 in isolated ISCs from Lsr^{ctrl} and $Lsr^{vill\ KO}$ mice (n=3). (D) YAP ubiquitination levels and quantification analysis in isolated ISCs from Lsr^{ctrl} and $Lsr^{vill\ KO}$ mice. Ubiquitinated YAP was first immunoprecipitated with anti-YAP antibody or anti-p-YAP (S381) antibody and then detected with anti-ubiquitin antibody

1028 (n=3). (E) Mass spectrometry analysis of LSR immunocomplexes precipitated from isolated ISCs. (F)
1029 Co-IP showing that endogenous YAP, LSR, and 14-3-3 zeta interacts with each other in isolated ISCs
1030 from Lsr^{ctrl} mice. (G) Co-IP showing that endogenous YAP interacts with endogenous LSR, but not
1031 PP2Ac in isolated ISCs from Lsr^{ctrl} mice. (H) Co-IP showing that endogenous YAP interacts with
1032 endogenous PP2Ac, but not 14-3-3 zeta in isolated ISCs from $Lsr^{vill\ KO}$ mice. (I) Western blot and
1033 quantification analysis of YAP and Ser381-phosphorylated YAP in HEK293 cells transfected YAP alone
1034 or together with PP2Ac (n=3). For all IP or Co-IP analysis, antibodies used for immunoprecipitation are
1035 shown above the lanes; antibody for blot visualization is shown on the right. $^{*}P < 0.05$, $^{**}P < 0.01$,
1036 $^{***}P < 0.001$.
1037

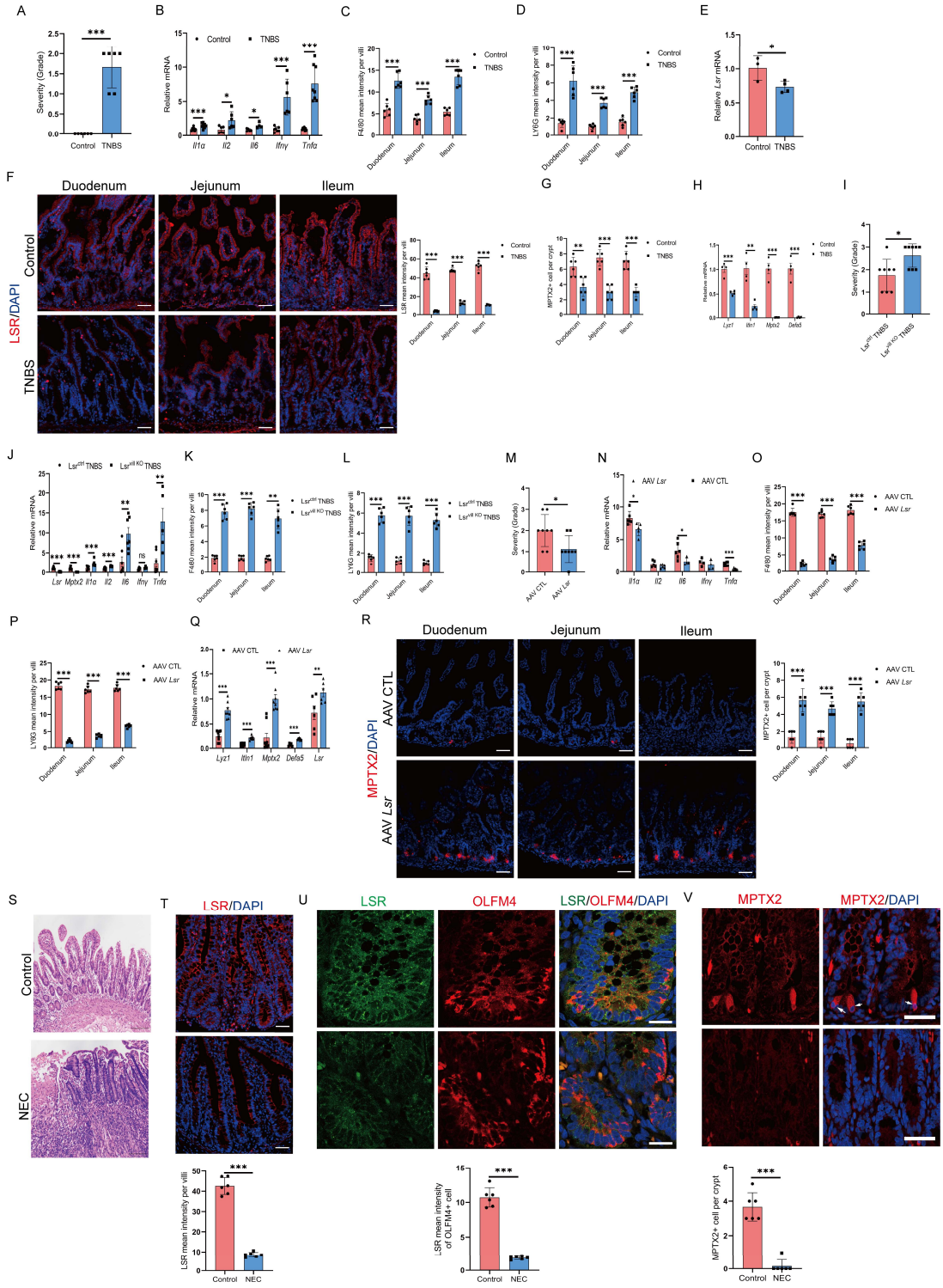

Fig. 6. Loss of *Lsr* exacerbates inflammation in a mouse model of NEC.

(A) Severity of intestinal injury in control and TNBS-treated mice (n=8). (B) Expression of *Il1α, Il2, Il6, Ifnγ* and *Tnfα* mRNA assessed by qRT-PCR in small intestines from control and TNBS-treated mice (n=8). (C and D) Quantification analysis of F4/80 (C) and LY6G (D) mean intensity per villi in small intestines from control and TNBS-treated mice (n=6). (E) Expression of *Lsr* mRNA assessed by qRT–PCR in small

intestines from control and TNBS-treated mice (n=4). (F) LSR immunofluorescence and quantification analysis in small intestines from control and TNBS-treated mice (n=6). (G) Quantification analysis of MPTX2^{+} cell per crypt in small intestines from control and TNBS-treated mice (n=6). (H) Expression of *Lyz1, Itln1, Mptx2* and *Defa5* mRNA assessed by qRT-PCR in small intestines from control and TNBS-treated mice (n=8). (I) Severity of intestinal injury in TNBS-treated Lsr^{ctrl} and Lsr$^{vill\ KO}$ mice (n=8). (J) Expression of *Lsr, Mptx2, Il1α, Il2, Il6, Ifnγ* and *Tnfα* mRNA assessed by qRT–PCR in small intestines from TNBS-treated Lsr^{ctrl} and Lsr$^{vill\ KO}$ mice (n=8). (K and L) Quantification analysis of F4/80 (K) and LY6G (L) mean intensity per villi in small intestines from TNBS-treated Lsr^{ctrl} and Lsr$^{vill\ KO}$ mice (n=6). (M) Severity of intestinal injury in TNBS-treated mice administered with AAV-CTL or AAV-Lsr (n=8). (N) Expression of *Il1α, Il2, Il6, Ifnγ* and *Tnfα* mRNA assessed by qRT–PCR in small intestines from TNBS-treated mice administered with AAV-CTL or AAV-Lsr (n=8). (O and P) Quantification analysis of F4/80 (O) and LY6G (P) mean intensity per villi in small intestines from TNBS-treated mice administered with AAV-CTL or AAV-Lsr (n=6). (Q) Expression of *Lyz1, Itln1, Mptx2, Defa5* and *Lsr* mRNA assessed by qRT–PCR in small intestines from TNBS-treated mice administered with AAV-CTL or AAV-Lsr (n=8). (R) MPTX2 immunofluorescence and quantification analysis in small intestines from TNBS-treated mice administered with AAV-CTL or AAV-Lsr (n=6). (S) Representative H&E-stained small intestinal biopsy specimens of subjects with NEC and a control. (T-V) LSR (T), LSR and OLFM4 (U), and MPTX2 (V) immunofluorescence and quantification analysis in small intestinal biopsy specimens of subjects with NEC and a control (arrows indicated Paneth cells) (n=6). Scale bars: F, R, T and V, 50 μm; S, 100 μm; U, 20 μm. $^{*}P < 0.05$, $^{**}P < 0.01$, $^{***}P < 0.001$.

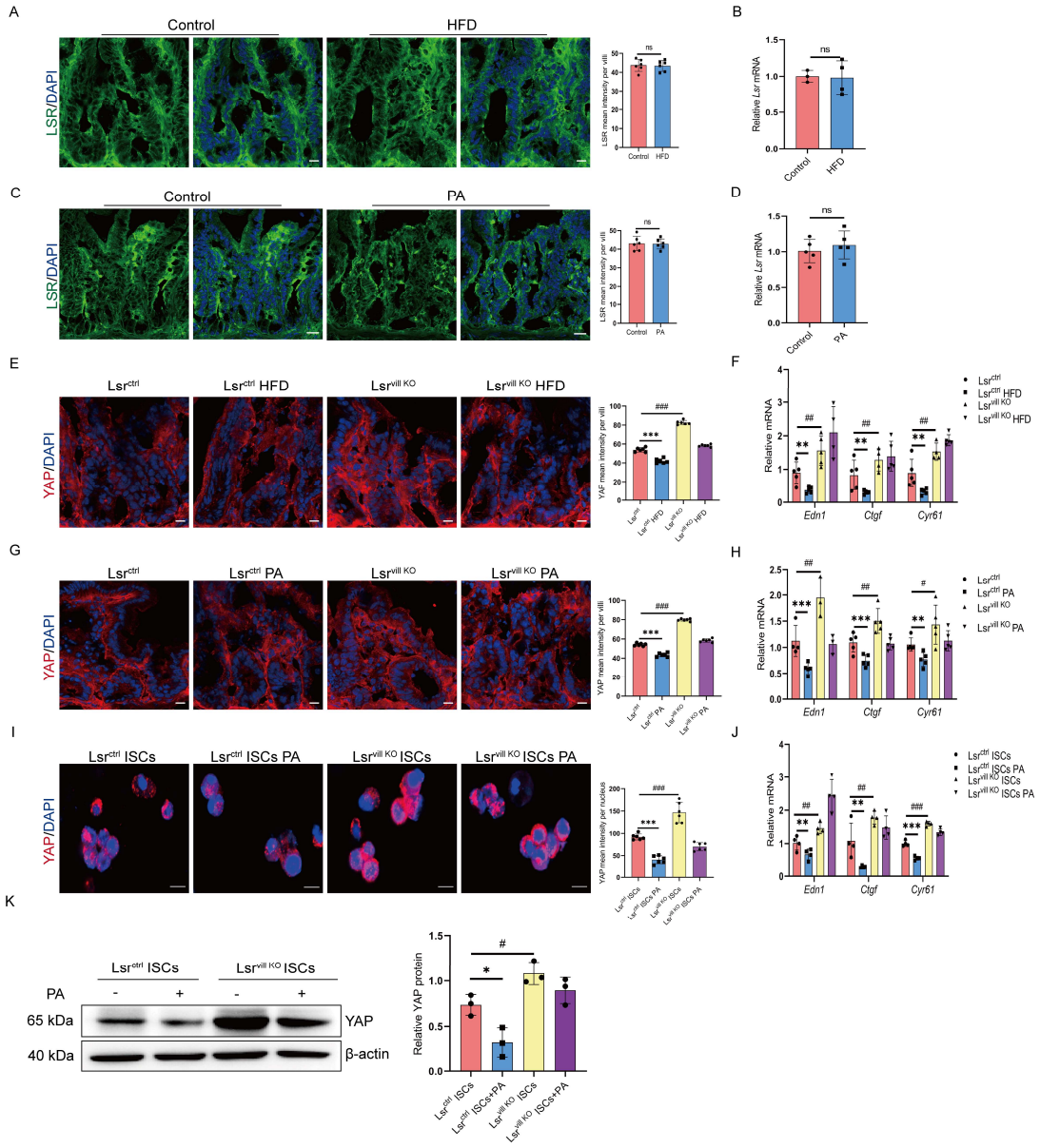

Fig. 7. LSR mediates the inhibitory effect of PA on YAP.

(A) LSR immunofluorescence and quantification analysis in small intestines from control or HFD-fed mice (n=6). (B) qRT–PCR analysis in small intestines from control or HFD-fed mice (n=5). (C) LSR immunofluorescence and quantification analysis in small intestines from vehicle control or PA-treated mice (n=6). (D) qRT–PCR analysis in small intestines from vehicle control or PA-treated mice (n=5). (E) YAP immunofluorescence and quantification analysis in small intestines from control or HFD-fed Lsr^{ctrl} and $Lsr^{vill\ KO}$ mice (n=6). (F) Expression of *Edn1, Ctgf* and *Cyr61* mRNA assessed by qRT–PCR in small intestines from control or HFD-fed Lsr^{ctrl} and $Lsr^{vill\ KO}$ mice (n=5). (G) YAP immunofluorescence and quantification analysis in small intestines from Lsr^{ctrl} and $Lsr^{vill\ KO}$ mice treated with vehicle control or

1075 PA (n=6). (H) Expression of *Edn1, Ctgf* and *Cyr61* mRNA assessed by qRT–PCR in small intestines
1076 from Lsr^{ctrl} and $Lsr^{vill\ KO}$ mice treated with vehicle control or PA. (n=5). (I) YAP immunofluorescence
1077 and quantification analysis in ISCs isolated from small intestine of Lsr^{ctrl} and $Lsr^{vill\ KO}$ mice treated with
1078 vehicle control or PA (n=6). (J) Expression of *Edn1, Ctgf* and *Cyr61* mRNA assessed by qRT–PCR in
1079 ISCs isolated from small intestine of Lsr^{ctrl} and $Lsr^{vill\ KO}$ mice treated with vehicle control or PA. (n=3).
1080 (K) Western blot and quantification analysis for YAP of ISCs lysates from small intestine of Lsr^{ctrl} and
1081 $Lsr^{vill\ KO}$ mice treated with vehicle control or PA (n=3). Scale bars: A, E, G and I, 10 μm; C, 20 μm. $^{*}P < 0.05$, $^{**}P < 0.01$, $^{***}P < 0.001$, $^{\#}P < 0.05$, $^{\#\#}P < 0.01$, $^{\#\#\#}P < 0.001$.